nature chemistry

Article

https://doi.org/10.1038/s41557-024-01557-2

Fast and facile synthesis of amidine-incorporated degradable lipids for versatile mRNA delivery in vivo

Received: 26 October 2022

Accepted: 14 May 2024

Published online: 09 July 2024

Check for updates

Xuexiang Han[1,2,15], Mohamad-Gabriel Alameh[3,4,5,15], Ningqiang Gong[1,15], Lulu Xue[1,15], Majed Ghattas[3], Goutham Bojja[3], Junchao Xu[1], Gan Zhao[6], Claude C. Warzecha[7], Marshall S. Padilla[1], Rakan El-Mayta[1,3], Garima Dwivedi[3], Ying Xu[8], Andrew E. Vaughan[6], James M. Wilson[7], Drew Weissman[3,4] ✉ & Michael J. Mitchell[1,4,9,10,11,12,13,14] ✉

Lipid nanoparticles (LNPs) are widely used for mRNA delivery, with cationic lipids greatly affecting biodistribution, cellular uptake, endosomal escape and transfection efficiency. However, the laborious synthesis of cationic lipids limits the discovery of efficacious candidates and slows down scale-up manufacturing. Here we develop a one-pot, tandem multi-component reaction based on the rationally designed amine–thiol–acrylate conjugation, which enables fast (1 h) and facile room-temperature synthesis of amidine-incorporated degradable (AID) lipids. Structure–activity relationship analysis of a combinatorial library of 100 chemically diverse AID-lipids leads to the identification of a tail-like amine–ring-alkyl aniline that generally affords efficacious lipids. Experimental and theoretical studies show that the embedded bulky benzene ring can enhance endosomal escape and mRNA delivery by enabling the lipid to adopt a more conical shape. The lead AID-lipid can not only mediate local delivery of mRNA vaccines and systemic delivery of mRNA therapeutics, but can also alter the tropism of liver-tropic LNPs to selectively deliver gene editors to the lung and mRNA vaccines to the spleen.

Messenger RNA (mRNA)-based therapeutics hold great promise to prevent and treat a variety of diseases[1,2]. However, safe and efficient delivery of mRNA-based vaccines and therapeutics to target tissues remains challenging[3]. Lipid nanoparticles (LNPs) represent the most clinically advanced non-viral nucleic acid delivery system, with one approved small interfering RNA (siRNA)-delivering DLin-MC3-DMA (MC3) LNP (Onpattro) and two approved mRNA vaccine-delivering SM-102 and ALC-0315 LNPs (BNT162b2 and mRNA-1273; Supplementary Table 1)[4]. LNPs are generally composed of four components: cationic lipid, phospholipid, PEGylated lipid (PEG-lipid) and cholesterol[5]. Among these, the cationic lipid plays an essential role in protecting and transporting nucleic acids[6].

Cationic lipids typically consist of a cationic head and several lipophilic tails[7]. Common headgroups include amines (primary to quaternary), guanidine and *N*-heterocyclic groups[8], which are involved in binding with negatively charged mRNAs during LNP formulation and interacting with anionic membrane phospholipids during endosome trafficking[6]. Although permanently charged cationic lipids (for example, 1,2-dioleoyl-3-trimethylammonium propane, DOTAP) used to be widely utilized in LNPs, they have now largely been replaced by state-of-the-art ionizable cationic lipids (for example, MC3 and SM-102) because of the pH-dependent protonation properties, enhanced delivery efficiency and improved biocompatibility of the latter[1]. The lipid tails impact lipophilicity, fluidity, fusogenicity and biodegradability,

A full list of affiliations appears at the end of the paper. ✉e-mail: dreww@upenn.edu; mjmitch@seas.upenn.edu

thereby influencing the endosomal escape, potency and toxicity of LNPs[7]. Previous studies have suggested that branched tails that enable lipids to adopt a more cone-shaped structure are favourable for mRNA delivery[9,10]. Additionally, ester bond-bearing tails are highly recommended for in vivo applications owing to their degradability[9,11]. The structure of the cationic lipids is critical, as subtle changes (for example, one atom or group) greatly affect the cellular uptake, endosomal escape, tissue targeting, cellular tropism and potency of LNPs[9,12–14].

To find efficacious cationic lipids and study their structure–activity relationships (SARs), dozens or even hundreds of chemically divergent candidates are usually needed for comparison. For example, over 60 rationally designed cationic lipids were synthesized by standard organic chemistry and tested in vivo for years before elucidating valuable structural criteria and identifying the MC3 lipid that was later approved by the Food and Drug Administration (FDA) for siRNA delivery[15,16]. Alternatively, combinatorial chemistries, such as aza-Michael addition, the epoxide-mediated ring-opening reaction and Ugi multi-component reaction (MCR) have been utilized to accelerate these processes[14,17–19]. Despite the successful discovery of some efficacious lipids, these combinatorial chemistries are generally performed under harsh conditions for several days and typically yield non-degradable lipids[6,20]. Accordingly, there is still great interest in developing new combinatorial chemistries to rapidly generate structurally diverse cationic lipids and study SARs for guiding the design of the next generation of delivery materials and fulfil the broader applications of mRNA therapeutics[6]. We aim to develop synthetic methods that can enable facile synthesis of degradable cationic lipids within hours, without requiring harsh conditions or specialized instruments.

In this Article, we describe a one-pot tandem multi-component reaction (T-MCR) to enable fast and facile synthesis of amidine-incorporated degradable (AID) lipids. This T-MCR is based on rationally designed amine–thiol–acrylate conjugation between amines, Traut's reagent (2-iminothiolane hydrochloride) and alkyl acrylates (Fig. 1). Mechanistically, a primary amine (a weak nucleophile) is rapidly converted to a basic amidine through the nucleophilic ring-opening of 2-iminothiolane, generating a thiol (a strong nucleophile) in situ, which immediately reacts with acrylate via Michael addition to afford the AID-lipid. The simplicity of T-MCR enabled us to synthesize 100 chemically diverse AID-lipids within 1 h at room temperature (r.t.). Through the investigation of SARs, we identified a tail-like amino head–ring-alkyl aniline that generally produces efficacious AID-lipids. Mechanistic studies demonstrated that the bulky benzene ring enhances membrane disruption and endosomal escape by assisting the AID-lipid to adopt a more conical shape. Our lead AID-lipid, 12T-O14, mediated efficient intramuscular (i.m.) delivery of mRNA vaccines and systemic delivery of mRNA therapeutics without noticeable toxicity. Moreover, we demonstrated that 12T-O14 serves as a superior supplementary lipid to redirect liver-tropic LNPs to selectively target the lung or spleen via simple adjustment of the formulation, which enabled CRISPR/Cas9-mediated gene editing in the lung and mRNA vaccine delivery to the spleen.

Results

Optimization of T-MCR for AID-lipid synthesis

To confirm the feasibility of the amine–thiol–acrylate conjugation, a model reaction between amine 19, Traut's reagent and acrylate **O12** was performed (Supplementary Fig. 1a). Several synthetic conditions were tested, and the reaction progress was monitored by liquid chromatography–mass spectrometry (LC-MS; Supplementary Fig. 1b,c). The reaction proceeded quickly at r.t. in the presence of the base triethylamine (TEA) in either dimethyl sulfoxide or ethanol (EtOH), with minimum by-products, and was complete in 1 h, with isolation yields of over 80% for the target product 19T-O12. Because the conversion of the primary amine to the thiolated product by Traut's reagent is typically complete within 1 h and the subsequent nucleophilic thiol-Michael addition proceeds instantly[21], the combination of these two reactions in a one-pot profile greatly simplifies and accelerates the synthetic process. Such a fast and mild synthesis, to our knowledge, has not been reported for previous combinatorial chemistries[6,20,22].

High-throughput synthesis and screening of AID-lipids

Next, we applied this T-MCR to synthesize a series of AID-lipids. EtOH was selected as the solvent, as it is a green solvent, and the resulting solution is ready for LNP formulation. Twenty-five amines, including alkylamines, anilines and hydrazides, were reacted in a combinatorial manner with four alkyl acrylates (**O9**, **O12**, **O14** and **O16**) to form 100 AID-lipids containing amidine and ester linkages (Fig. 1a). To enable fast and high-throughput synthesis, individual reactions were performed in 1.5-ml Eppendorf tubes, and all tubes were sonicated simultaneously for 1 h (Fig. 2a).

The resulting 100 AID-lipids were formulated into 100 AID-LNPs along with excipients including 1,2-dioleoyl-*sn*-glycero-3-phosphoethanolamine (DOPE), cholesterol and 1,2-dimyristoyl-rac-glycero-3-methoxypolyethylene glycol-2000 (DMG-PEG). To evaluate the mRNA delivery efficacy of this lipid library and study the SARs, 1-methyl-pseudouridine (m1ψ)-modified luciferase mRNA (mLuc) was encapsulated into these LNPs, and luciferase protein expression in HepG2 cells was determined. Of the 100 AID-lipid members, none showed toxicity (cell viability <80%; Supplementary Fig. 2). Moreover, 98 AID-lipids were able to deliver mRNA in vitro (Fig. 2b,c). Of these, 23 mediated luciferase expression of up to 100,000 units (considered as outstanding performance). Analysis of these 23 outstanding AID-lipids showed that they were synthesized by long-chain (C_{14}–C_{18}) alkylamines, ring-alkyl anilines, diamines or partial polyamines (Fig. 2d), whose relative hit rates (percentage in the group with luminescence >100,000 units − percentage in library) were 10.1, 14.1, 9.7 and −5.9, respectively (Fig. 2e). Although monoamines, overall, were inferior in affording outstanding AID-lipids (relative hit rate = −3.8), two monoamine subclasses (long-chain alkylamine and ring-alkyl anilines) generally yielded outstanding AID-lipids (Fig. 2e). Interestingly, ring-alkyl anilines tended to generate more potent AID-lipids (luminescence of >200,000 units) compared to long-chain alkylamines, despite having the same number of carbon atoms (for example, 12T-O14 versus 4T-O14; 13T-O14 versus 5T-O14; Fig. 2c). With respect to tail length, **O14** generally outperformed others to produce efficacious AID-lipids with the highest relative hit rate of 9.8 (Fig. 2f).

Because ring-alkyl aniline has the highest hit rate, and such structures (either as amino heads or as tails) have never been reported as efficacious building blocks in previous combinatorial libraries, we focused on this family of AID-lipids. It is noteworthy that anilines **11**–**14** not only provide a primary amine for amidine formation, but also constitute one of the two tails in the corresponding asymmetric AID-lipids. Therefore, the length and hydrophobicity of the alkyl substituent on the benzene ring should greatly impact mRNA delivery. Indeed, elongation of the alkyl substituent appeared to increase delivery efficiency (**11**–**13**; Fig. 2c and Supplementary Fig. 3), but replacement of one carbon with the polar oxygen atom in the alkyl substituent dramatically decreased efficacy, presumably due to its reduced hydrophobicity (**12** versus **14**; Supplementary Fig. 4).

We next explored the in vivo delivery efficacy of AID-lipids. The top eight AID-lipid candidates (luminescence of >200,000 units) from the in vitro screening were tested in mice after i.m. injection. Despite all AID-LNPs showing similar in vitro potency and achieving strong transfection at an mRNA dose as low as 3.7 ng per well (Fig. 2g), their in vivo performance was disparate (Fig. 2h). Two AID-lipids, 12T-O14 and 13T-O14, mediated substantially higher mLuc transfection than the others. Interestingly, both possess a ring-alkyl aniline and an **O14** tail, correlating well with their high relative hit rates (Fig. 1e,f). We purified a few AID-lipids and confirmed the consistency of their in vivo performance with their crude ones, as well as the superiority of the ring-alkyl aniline (that is, **12** and **13**) and **O14** tail (Supplementary Fig. 5). Furthermore,

https://doi.org/10.1038/s41557-024-01557-2

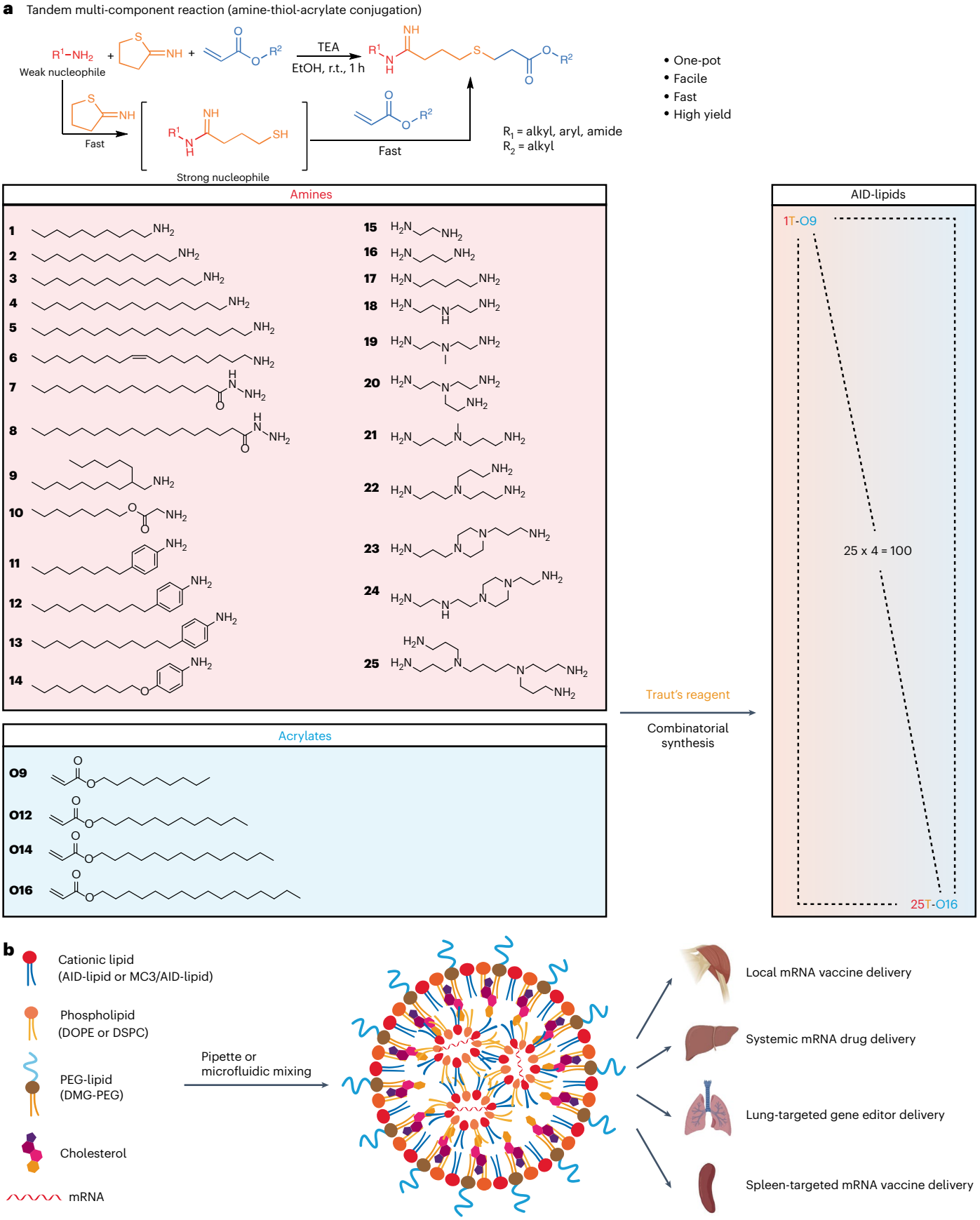

Fig. 1 | Fast and facile synthesis of AID-lipids via T-MCR for mRNA delivery. **a**, T-MCR based on amine–thiol–acrylate conjugation between amines, Traut's reagent and alkyl acrylates. The reaction scheme and mechanism of T-MCR, as well as the chemical structures of amines **1**–**25** and alkyl acrylates **O9**–**O16** are shown. **b**, Scheme of the formulation and application of mRNA-loaded LNPs. AID-lipid-formulated LNPs mediate delivery of mRNA-based vaccines as well as protein replacement and gene-editing therapeutics to target tissues. The schematic in **b** was created with BioRender.com.

https://doi.org/10.1038/s41557-024-01557-2

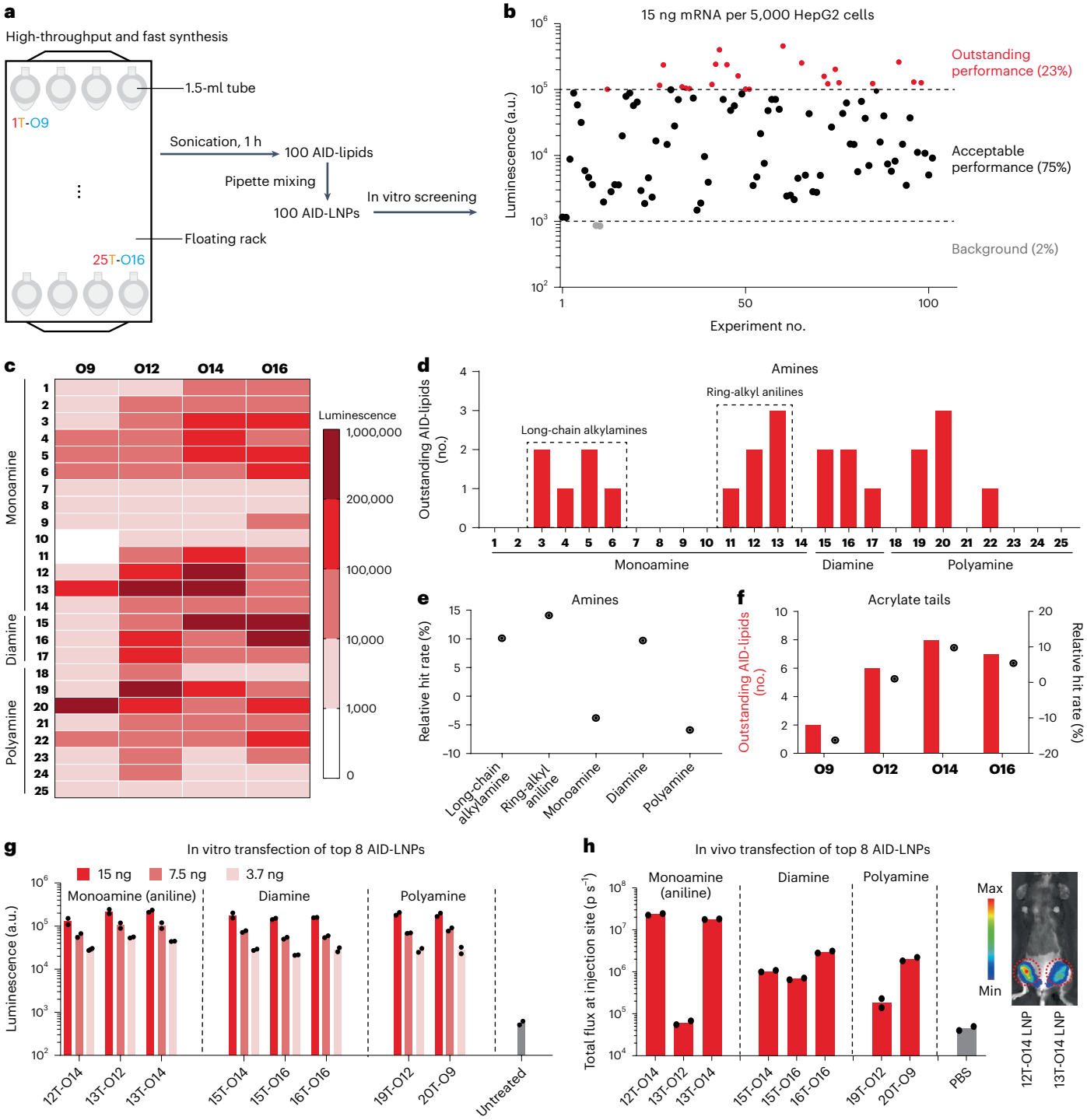

Fig. 2 | High-throughput synthesis and screening of AID-lipids. a, Fast and high-throughput synthesis of 100 AID-lipids. All reactions were performed separately and simultaneously in 1.5-ml Eppendorf tubes using ultrasound-mediated mixing for 1 h. **b**, AID-LNPs mediated mLuc transfection in vitro ($n = 2$ biologically independent samples, initial screening). mLuc-loaded AID-LNPs were formulated by pipette mixing and used to transfect HepG2 cells at a dose of 15 ng mRNA per well for 24 h. The performance was evaluated based on luminescence readout (>100,000 units, outstanding; 1,000–100,000 units, acceptable). **c**, Luciferase expression as a heatmap. **d**, Distribution of outstanding AID-lipids based on amines. **e**, Analysis of relative hit rates (percentage in the group with >100,000 units – percentage in library) based on amine subclasses. **f**, Distribution of outstanding AID-lipids and analysis of relative hit rates based on acrylate tails. **g**, The top eight AID-LNPs mediated dose-dependent mLuc transfection in vitro ($n = 2$ biologically independent samples, initial screening). HepG2 cells were treated with 3.7, 7.5 or 15 ng mRNA per well for 24 h. **h**, The top eight AID-LNPs mediated mRNA delivery in vivo ($n = 2$ biologically independent samples, initial screening). AID-LNPs were i.m. injected into mice (2 μg mLuc per injection) and the total flux of luminescence at the injection site was quantified at 4 h post treatment. A representative in vivo bioluminescence image is shown. Data are presented as means.

we customized two unsaturated acrylate tails (**O18a** and **O18b**; Supplementary Fig. 6), and then applied T-MCR to generate 12T-O18a and 12T-O18b. Despite their improved in vitro mRNA delivery efficiency compared to 12T-O14, neither achieved better in vivo performance. More comprehensive structural optimization of AID-lipids involving additional synthetic steps is still ongoing and will be reported in a future

study. Here, the top-performing AID-lipid, 12T-O14, was purified, characterized (Supplementary Figs. 7–9) and used for subsequent studies.

Optimization and characterization of AID-LNP

After acquiring the purified 12T-O14, we next systematically optimized the LNP formulation using an in vitro/vivo hybrid method (Supplementary Fig. 10), which resulted in a molar ratio of 12T-O14, cholesterol, DOPE and DMG-PEG of 33:48.5:17:1.5. Next, the physicochemical properties of the 12T-O14 LNP formulated by microfluidic mixing of lipids (in ethanol) and mRNA (in citrate buffer, pH 3.0) were characterized. The mRNA encapsulation efficiency (EE) of this LNP was 93.4%, suggesting its strong ability to condense and entrap mRNA molecules (Fig. 3a). The hydrodynamic diameter of 12T-O14 LNP was ~73.4 nm (Supplementary Fig. 11), with a low polydispersity index (PDI = 0.075) and a neutral surface charge (ζ = 1.63 mV). The apparent pK_a of the 12T-O14 LNP was determined to be 8.15 (Supplementary Fig. 12), suggesting that 12T-O14 is protonated at pH 7.4 due to the basicity of the amidine[23]. Owing to this feature, 12T-O14 LNP could also efficiently encapsulate mRNA through electrostatic interaction in neutral phosphate buffered saline (PBS) buffer with an EE of 88.1% (Fig. 3a). A representative cryogenic electron microscopy (cryo-EM) image showed that 12T-O14 LNP was spherical, with a multi-lamellar shell and an amorphous core (Fig. 3b).

AID-lipid enables safe and effective intracellular mRNA delivery

Previous studies have suggested that cationic lipids are prone to induce immunotoxicity and cytotoxicity[24,25]. We therefore compared the immunostimulatory effect of 12T-O14 LNP with a series of benchmark LNPs in RAW264.7 macrophages (Supplementary Fig. 13). Two proinflammatory cytokines, tumour necrosis factor-α (TNF-α) and interleukin-6 (IL-6), were examined by enzyme-linked immunosorbent assay (ELISA). 12T-O14 LNP induced marginal levels of TNF-α and undetectable levels of IL-6, which were comparable to those of DOTMA, DOTAP, MC3 and SM-102 LNPs but were substantially lower than for C12-200 LNP[18]. These results suggest that 12T-O14 LNP had a low immunostimulatory effect. We next investigated the cytotoxicity of 12T-O14 LNP in HepG2 cells (Fig. 3c). LNPs formulated by the traditional cationic lipid DOTAP and the state-of-the-art ionizable cationic lipid SM-102 were chosen for comparison. Our results showed that 12T-O14 LNP and SM-102 LNP were more biocompatible than DOTAP LNP, as DOTAP LNP greatly reduced cell viability at a high dose.

After confirming the low toxicity profile of 12T-O14 LNP, we next compared its intracellular mRNA delivery efficiency. 12T-O14 LNP outperformed DOTAP LNP in delivery of mLuc into HepG2 cells, although it was inferior to SM-102 LNP (Fig. 3d). In terms of siRNA delivery, 12T-O14 LNP mediated greater gene knockdown than DOTAP LNP, which was comparable to the gold-standard siRNA-delivering system MC3 LNP (Supplementary Fig. 14). These results suggest that 12T-O14 LNP is able to efficiently deliver different RNA constructs into cells.

AID-lipid uses a benzene ring to aid membrane disruption

Endosomal entrapment of LNPs is a critical barrier for intracellular mRNA delivery[26,27]. Therefore, the superior performance of 12T-O14 LNP prompted us to investigate its endosomal escape properties. Confocal laser scanning microscope (CLSM) images showed that, similar to SM-102 LNP, 12T-O14 LNP escaped from endosomes more efficiently than DOTAP LNP (Fig. 3e), as a greater cytosolic distribution of LNPs (green) and less co-localization between LNPs and endosomes (red) were observed in 12T-O14 LNP-treated cells. We noticed that a major structural difference between 12T-O14 and DOTAP (or many other AID-lipids) is that the former bears a benzene ring, so we hypothesized that this bulky group could act as a wedge that increases the distance between two tails to produce a cone shape (the 'wedge effect'; Fig. 3f), which can form a more cone-shaped ion pair with the anionic membrane phospholipid to enhance endosome disruption[6]. To verify this hypothesis, the packing parameter p of the lipid molecule was calculated based on molecular dynamics simulations (Fig. 3g,h), and was found to be correlated to the cone angle from the polar head to terminal tails[28]. For a more rigid comparison, 4T-O14, which contains a C_6 aliphatic chain instead of a benzene ring, was included (Fig. 3f). Our calculation found that the p value of 12T-O14 (p = 4.71) was larger than that of 4T-O14 (p = 4.11), DOTAP (p = 2.03) and SM-102 (p = 3.60). These computational results suggest that 12T-O14 possesses a more cone-shaped structure and is more likely to induce the rupture of endosomal membranes.

We next evaluated the membrane-disruptive activities of these lipids using a haemolysis assay (Fig. 3i). 12T-O14 LNP exhibited much stronger haemolysis than 4T-O14 LNP, DOTAP LNP and SM-102 LNP at pH 7.4 (Fig. 3h). Notably, similar to SM-102 LNP, the haemolytic activity of 12T-O14 LNP was enhanced at acidic pH, suggesting that the bulky benzene ring (to produce a cone-shaped structure) and the cationic amidine (to bind with the anionic membrane phospholipid) cooperatively contribute to membrane disruption. It is worth mentioning that the strong haemolytic activity of 12T-O14 LNP at neutral pH was reduced in the presence of serum (Supplementary Fig. 15), indicating that improved haemocompatibility is achieved after protein absorption[29]. Together, these results demonstrate the importance of the benzene ring in facilitating the endosomal escape of 12T-O14 LNP.

Local mRNA vaccine delivery and systemic mRNA drug delivery

Inspired by the synthetic simplicity, in vitro potency, marginal immunotoxicity and low cytotoxicity of 12T-O14, we further explored its potential for vaccine and protein replacement therapy development by delivering functional mRNAs in vivo. DOTAP and SM-102 were chosen for comparison due to their prevalence in the delivery of mRNA vaccines and therapeutics[30–33]. Local administration of LNP-formulated mRNA encoding antigen has been widely adopted for vaccination to trigger antigen-specific antibodies in both preclinical and clinical settings. After confirming that 12T-O14 LNP mediated greater protein expression than DOTAP LNP, but less protein expression than SM-102 LNP, following i.m. injection of mLuc-loaded LNPs (Fig. 4a), we tested the antibody responses of SARS-CoV-2 Spike mRNA-encapsulated LNP vaccines (Fig. 4b). We measured anti-Spike-specific binding immunoglobulin G (IgG) in mice following a prime and boost immunization regimen. The results showed that, in five mice receiving 12T-O14 LNP

Fig. 3 | Characterization and in vitro evaluation of 12T-O14 LNP. **a**, Characterization of 12T-O14 LNP (n = 3 biologically independent samples). 12T-O14 LNPs were formulated either in citrate buffer (10 mM, pH 3.0) or PBS buffer (10 mM, pH 7.4). **b**, Representative cryo-EM image of 12T-O14 LNP. Scale bar, 50 nm. **c**, Cytotoxicity of LNPs (n = 3 biologically independent samples). HepG2 cells were treated with the indicated mRNA dose for 24 h. The dashed line indicates 80% cell viability. **d**, LNPs mediated mLuc transfection in vitro (n = 3 biologically independent samples). HepG2 cells were treated with the indicated mRNA dose for 24 h. **e**, Representative CLSM images of cellular uptake. HepG2 cells were treated with DiO-labelled LNPs for 2 h before staining with LysoTracker Deep Red and Hoechst 33342 for imaging. Scale bars, 20 μm. **f**, Chemical structures of cationic lipids and the proposed mechanism of benzene ring-mediated cone-shape formation. 12T-O14 adopts a more conical shape due to the existence of the bulky benzene ring, which acts as a wedge to increase the distance between the two tails. Consequently, 12T-O14 forms a more cone-shaped ion pair with the anionic membrane phospholipid, which can enhance endosome disruption. **g**, Structural illustration of cationic lipids. **h**, Critical packing parameters of cationic lipids calculated based on molecular dynamics simulations. **i**, Haemolysis of LNPs at pH 7.4 or 6.0 (n = 3 biologically independent samples). RBCs were incubated with LNPs at 37 °C for 1 h before the supernatant was transferred into a clear 96-well plate (left) to determine the absorption at 540 nm (right). Data are presented as mean ± s.d. In **c**, **d** and **i**, one-way ANOVA with Tukey's correction was used.

https://doi.org/10.1038/s41557-024-01557-2

vaccine, one mouse (20%) responded after priming, and all mice (100%) responded after boosting, which was similar to the SM-102 LNP vaccine and outperformed the DOTAP LNP vaccine, for which no mice responded (0%) after priming and only two mice responded (40%) after boosting. Moreover, the average anti-Spike IgG titre in 12T-O14 LNP-vaccinated mice reached 4.7×10^5, which was on par with that in SM-102 LNP-vaccinated mice and 1,161-fold higher than that in DOTAP LNP-vaccinated mice. We further measured neutralization antibodies (NAbs) against a SARS-CoV-2 pseudovirus using a lentivirus-based pseudovirus neutralization assay (Supplementary Fig. 16). The 12T-O14 LNP vaccine triggered a much higher titre of NAbs than DOTAP LNP vaccine, although it was slightly inferior to the SM-102 LNP vaccine. These results suggest that 12T-O14 LNP could be a promising vector for local mRNA vaccine delivery.

a

LNP	12T-O14 LNP	
Ethanolic (lipid) phase	12T-O14 LNP:DOPE:Chol:DMG-PEG (33:17:48.5:1.5)	
Aqueous (mRNA) phase	Citrate buffer, pH 3.0	PBS buffer, pH 7.4
Diameter (nm)	73.4 ± 1.6	93.1 ± 1.2
PDI	0.075	0.061
Zeta potential (mV)	1.63 ± 2.8	2.33 ± 3.2
EE (%)	93.4	88.1
pK_a	8.15	

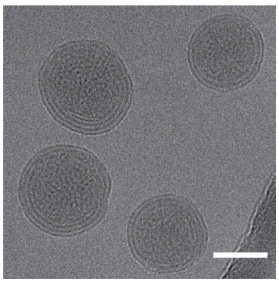

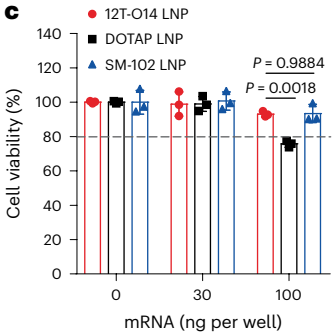

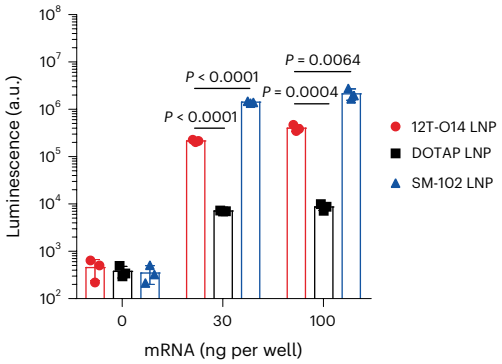

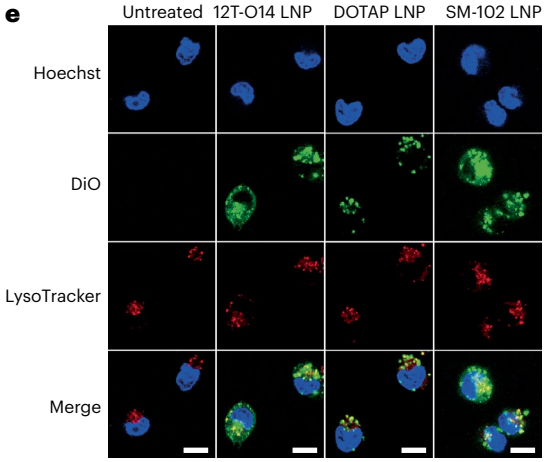

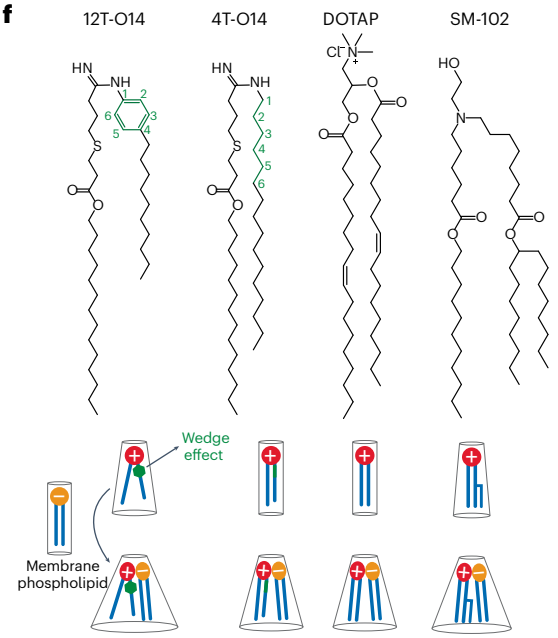

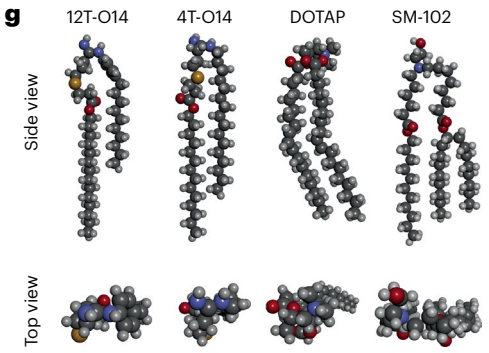

h

Packing parameters	12T-O14	4T-O14	DOTAP	SM-102
V	1231.21	1173.27	1413.98	1426.20
A	12.33	12.33	32.01	20.16
L	21.19	23.14	21.80	19.66
p value	4.71	4.11	2.03	3.60

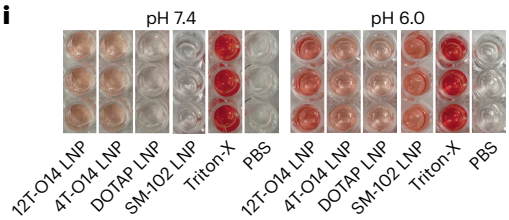

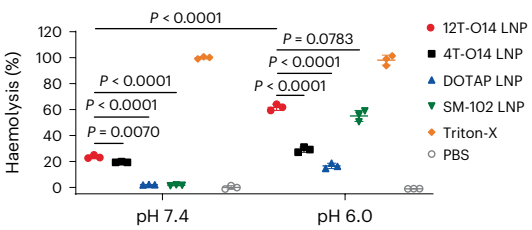

https://doi.org/10.1038/s41557-024-01557-2

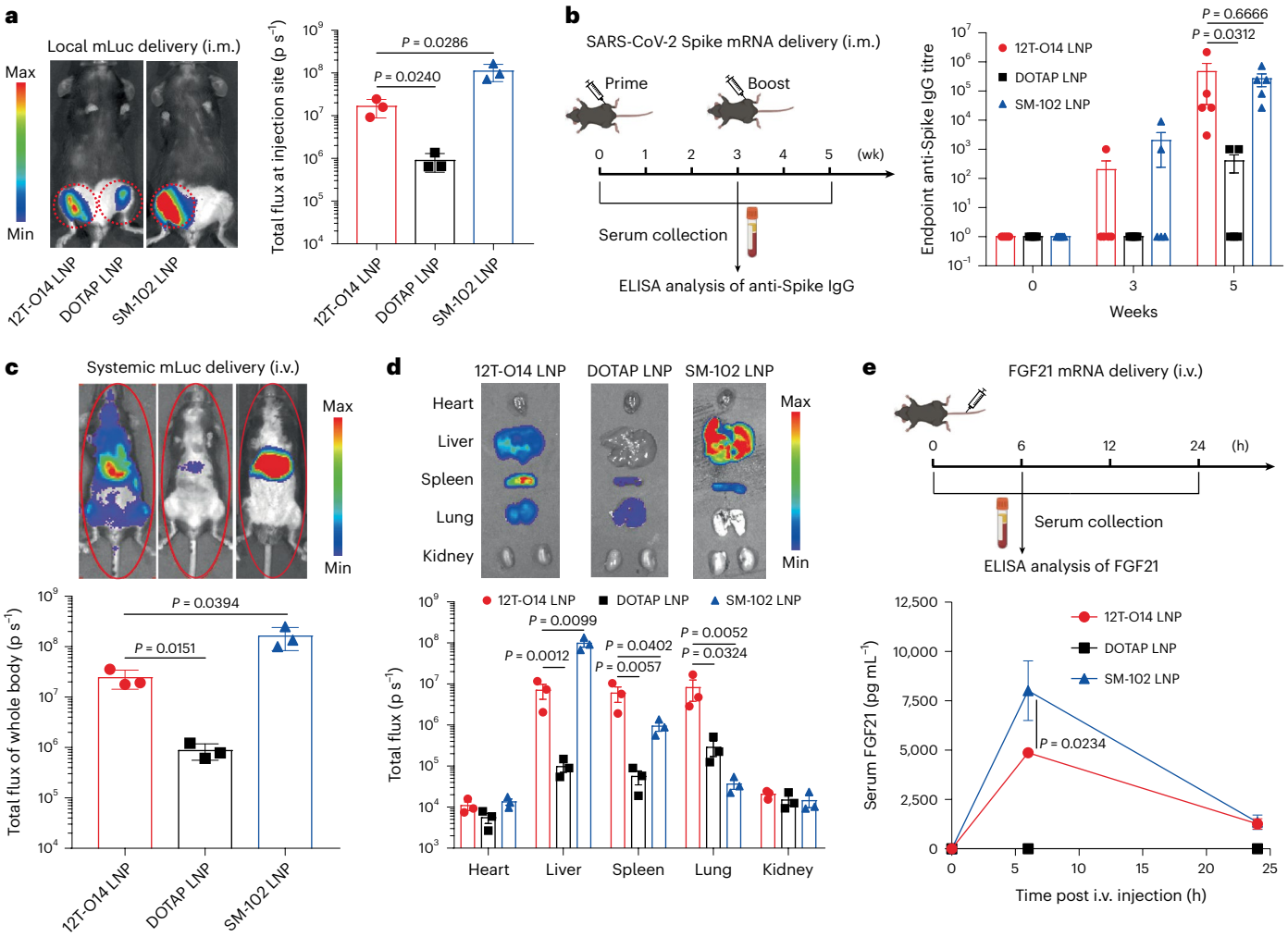

Fig. 4 | 12T-O14 enables local mRNA vaccine and systemic mRNA drug delivery. a, In vivo bioluminescence imaging of mice after LNP-mediated local mLuc delivery ($n = 3$ biologically independent samples). LNPs were i.m. injected into mice (2 μg mLuc/injection) and the total flux (photons per second (p s^{-1})) of luminescence at the injection site was quantified at 4 h post treatment. **b**, LNP-mediated SARS-CoV-2 Spike mRNA vaccine delivery ($n = 5$ biologically independent samples). Mice were i.m. vaccinated twice using a prime–boost strategy with a three-week interval. Anti-Spike IgG titres were determined by ELISA. **c**,**d**, In vivo (**c**) and ex vivo (**d**) bioluminescence imaging of mice after LNP-mediated systemic mLuc delivery ($n = 3$ biologically independent samples). LNPs were i.v. injected into mice (2 μg mLuc per mouse) and the total flux of whole body or excised organs was quantified at 4 h post treatment. **e**, LNP-mediated FGF21 mRNA delivery ($n = 3$ biologically independent samples). LNPs were i.v. injected into mice (5 μg mRNA per mouse), and serum FGF21 concentration was determined by ELISA. Data are presented as mean ± s.d. In **a**–**e**, one-way ANOVA with Tukey's correction was used. Schematic components in **b** and **e** were created with BioRender.com.

Next, we explored whether 12T-O14 LNP was able to deliver functional mRNA systemically, as systemic delivery of mRNA-encoding therapeutic proteins holds great potential to treat many diseases. First, the in vivo transfection profile was determined by examining luciferase expression following intravenous (i.v.) injection of mLuc-loaded LNPs. Whole body bioluminescence imaging showed that 12T-O14 LNP enabled 28-fold stronger luciferase expression than DOTAP LNP (Fig. 4c). Predominant transfection of liver, spleen and lung was observed in 12T-O14 LNP-treated mice (Fig. 4d), with a total flux 72-, 108- and 28-fold higher than that in DOTAP LNP-treated mice. We next tested the systemic delivery of mRNA encoding human fibroblast growth factor 21 (FGF21, a metabolic hormone primarily secreted by the liver), which is a promising therapeutic protein to treat obesity, type 2 diabetes and non-alcoholic steatohepatitis[34,35]. Although a high level of circulating FGF21 was detected in 12T-O14 LNP-treated mice at 6 h post treatment (Fig. 4e), none was detected in DOTAP LNP-treated mice due to its faint liver transfection. The state-of-the-art SM-102 LNP enabled stronger liver transfection and higher FGF21 expression than 12T-O14 LNP (Fig. 4c–e). We also analysed the toxicity of LNPs at 24 h post treatment. None of the three LNPs caused damage to the liver and other organs, as no obvious increases in alanine aminotransferase and aspartate aminotransferase, nor any histological abnormalities, were observed (Supplementary Fig. 17). Moreover, cytokine analysis revealed that all 13 cytokines tested were either undetectable or at low levels (< 5 pg ml^{-1}) for all three LNPs (Supplementary Table 2). These results indicate that 12T-O14 LNP can mediate systemic mRNA delivery for potential protein replacement therapy with good tolerability.

AID-lipid redirects liver-tropic LNPs to target lung or spleen

Although most LNPs tend to accumulate in the liver, there is a huge demand to develop LNP technologies for non-liver mRNA delivery, such as to the lung or spleen[36]. So far, however, very few studies have successfully engineered liver-tropic LNPs to switchably and selectively target the lung or spleen. Previous studies have indicated that manipulating the internal and/or external charge of LNP formulations can tune

https://doi.org/10.1038/s41557-024-01557-2

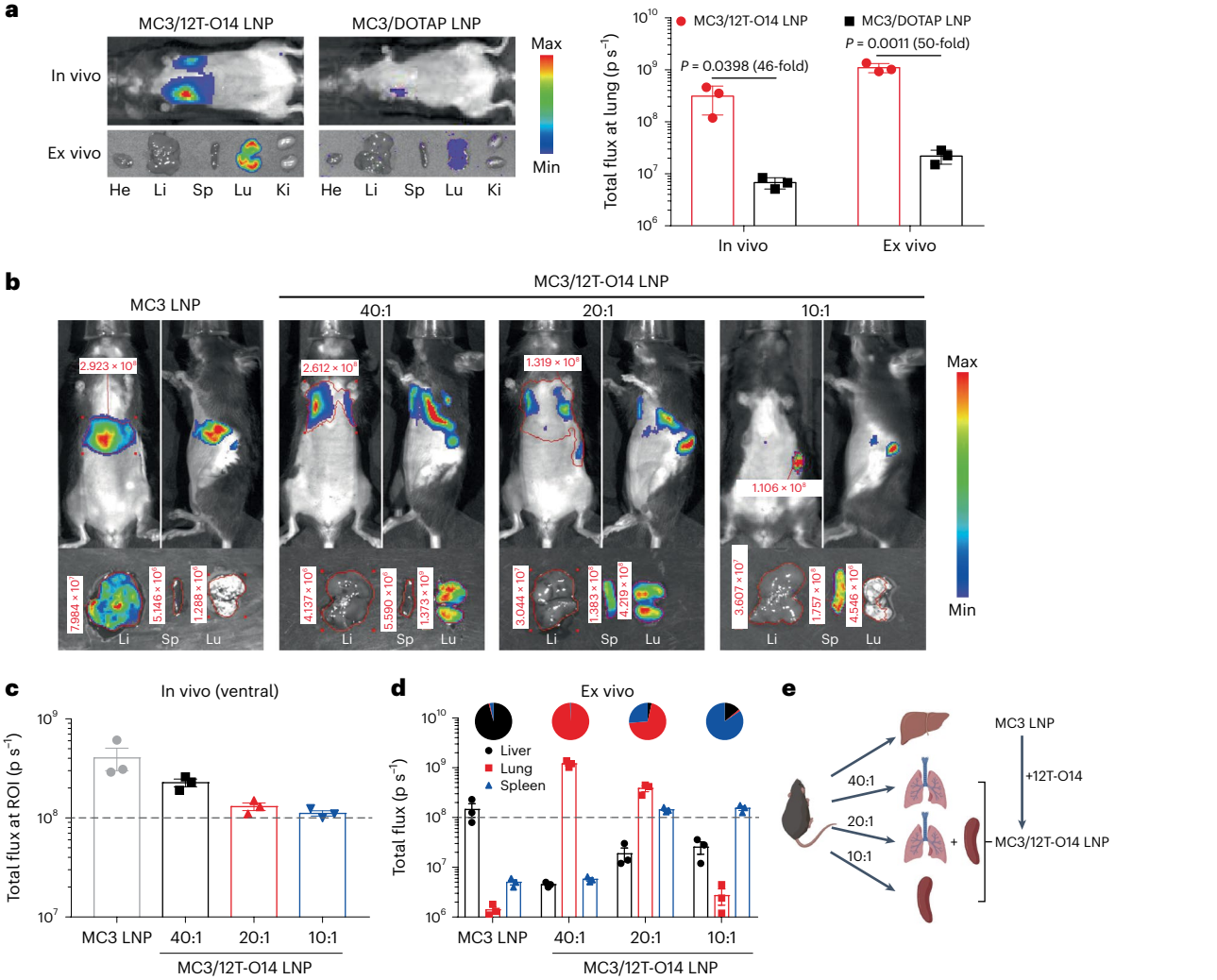

Fig. 5 | 12T-O14 redirects liver-tropic LNPs to selectively target lung or spleen. a, In vivo and ex vivo bioluminescence imaging (left) of mice treated with mLuc-loaded MC3/12T-O14 LNP or MC3/DOTAP LNP ($n = 3$ biologically independent samples). LNPs with a total lipids:mRNA weight ratio of 40:1 were i.v. injected into mice (2 μg mLuc per mouse), and the total flux of the lung was quantified at 4 h post treatment (right). He, heart; Li, liver; Sp, spleen; Lu, lung; Ki, kidney. **b**–**d**, In vivo (**b**,**c**) and ex vivo (**b**,**d**) bioluminescence imaging of mice treated with mLuc-loaded MC3/12T-O14 LNP ($n = 3$ biologically independent samples). LNPs with different total lipids:mRNA weight ratios were i.v. injected into mice (2 μg mLuc per mouse), and the total flux of the region of interest (ROI) was quantified at 4 h post treatment (**c**). In **c**, the total flux at the liver region for MC3 LNP, the lung region for MC3/12T-O14 LNP (40:1), the lung plus spleen region for MC3/12T-O14 LNP (20:1) and the spleen region for MC3/12T-O14 LNP (10:1) is plotted. MC3 LNP was used as a positive control for liver transfection. The dashed lines indicate a total flux of 1×10^8 p s^{-1}. **e**, Schematic illustration of 12T-O14 supplementation and lipids:mRNA weight ratio manipulation enabling selective lung and/or spleen transfection. Data are presented as mean ± s.d. In **a**, an unpaired two-tailed Student's *t*-test is used. Schematic components in **e** were created with BioRender.com.

organ tropism, known as selective organ targeting (SORT) technology[37]. We hypothesized that 12T-O14 could also be used as a supplementary cationic lipid to develop lung-targeted LNPs similar to the previously reported SORT LNP[37]. We chose an FDA-approved liver-tropic MC3 LNP as the framework formulation and supplemented it with 50% 12T-O14 to develop MC3/12T-O14 LNP (MC3:DSPC:cholesterol:DMG-PEG:12T-O14 = 25:5:19.25:0.75:50; Supplementary Table 3). The standard lung-tropic 50% DOTAP-supplemented MC3 SORT LNP (termed MC3/DOTAP LNP or lung-SORT LNP) was prepared accordingly and served as a positive control. The weight ratio of total lipids:mRNA was kept at 40:1 to ensure excess positive charge for both LNPs[37]. The in vivo and ex vivo imaging results showed that while both mLuc-loaded LNPs predominantly transfected the lungs (Fig. 5a), our MC3/12T-O14 LNP was ~50-fold more potent than MC3/DOTAP LNP. It is worth mentioning that very strong transfection was achieved in the lungs (total flux of $>1 \times 10^9$ p s^{-1}) by our MC3/12T-O14 LNP at a low mRNA dose (0.1 mg kg^{-1}), highlighting its potential for lung-targeted mRNA delivery.

Next, we explored whether 12T-O14 supplementation could redirect liver-tropic MC3 LNP to the spleen. Because negatively charged LNPs have been shown to preferentially target the spleen[37,38], we gradually decreased the weight ratio of total lipids:mRNA from 40:1 to 10:1 to obtain excess negative charge in MC3/12T-O14 LNP while keeping the lipid molar ratio unchanged. The decrease of weight ratio shifted the surface charge of MC3/12T-O14 LNP from slightly positive (40:1, 6.1 mV) to near-neutral (20:1, −1.2 mV) and finally to negative (10:1, −13.8 mV), without substantially reducing the mRNA EE (Supplementary Table 3). Correspondingly, the luciferase expression shifted from lung (40:1) to lung and spleen (20:1), and finally to spleen (10:1; Fig. 5b). Interestingly, while MC3 LNP predominantly transfected the liver with a luminescence flux above 1×10^8 p s^{-1}, 12T-O14 supplementation almost completely shifted the transfection to lung and/or spleen with designated fluxes maintained above 1×10^8 p s^{-1} (Fig. 5c,d). Notably, although lung and spleen can both be transfected by 12T-O14 LNP as previously shown (Fig. 4d), this 12T-O14 supplementation strategy can enable much

https://doi.org/10.1038/s41557-024-01557-2

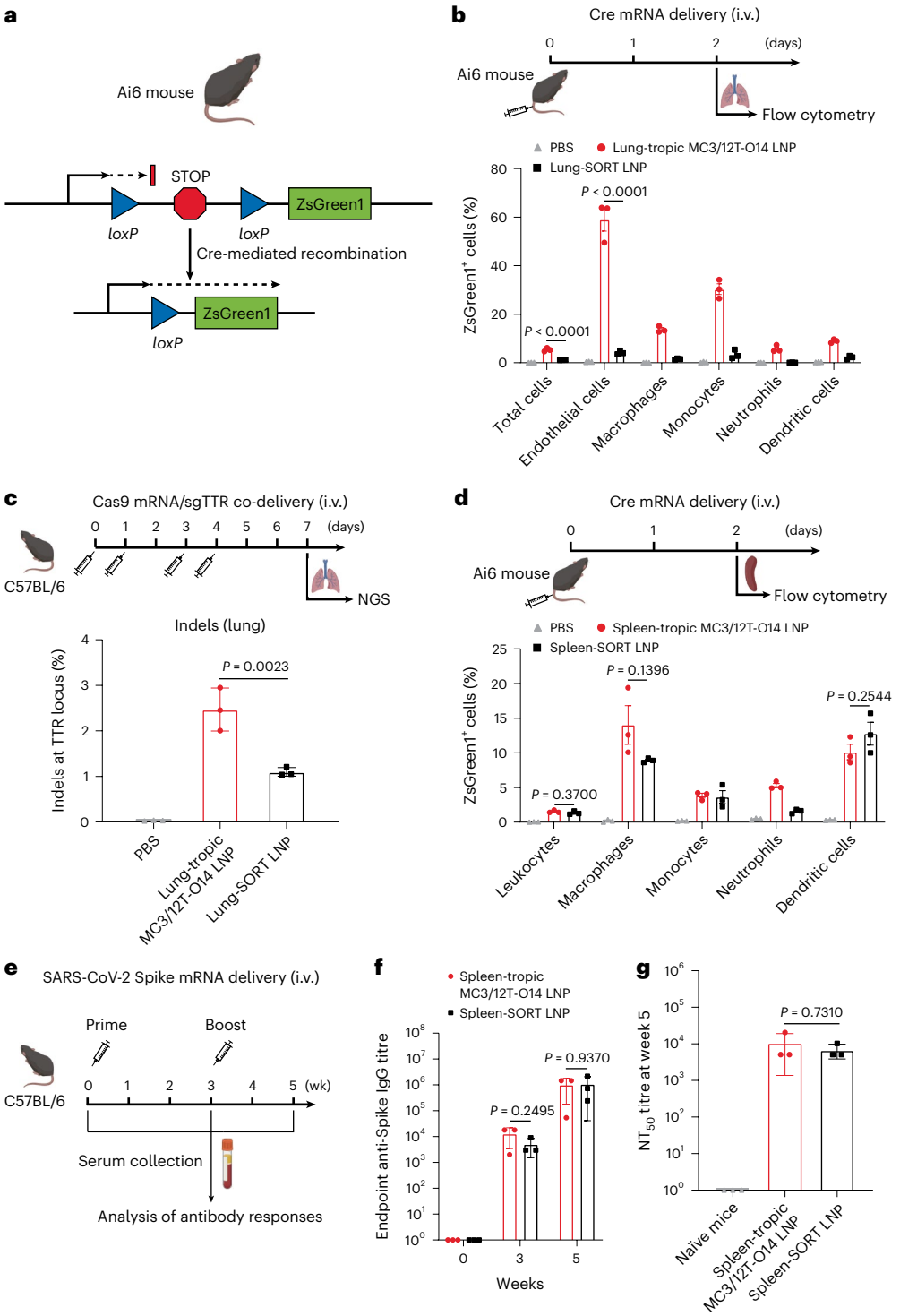

Fig. 6 | 12T-O14 redirects liver-tropic LNPs to deliver functional mRNAs to non-liver cells. a, Schematic illustration of Cre-mediated genetic recombination to turn on ZsGreen1 in Ai6 mice. **b**, Flow cytometry analysis of ZsGreen1$^+$ cells within defined cell-type populations of the lung after Cre mRNA delivery ($n = 3$ biologically independent samples). Cre mRNA (5 μg per mouse) was delivered into Ai6 mice by lung-tropic MC3/12T-O14 LNP or lung-SORT LNP via i.v. injection. On day 2, mice were euthanized and lungs were collected for analysis. **c**, CRISPR/Cas9-mediated gene editing in the lung ($n = 3$ biologically independent samples). Cas9 mRNA and sgTTR (4:1, wt:wt) were co-delivered into C57BL/6 mice by lung-tropic MC3/12T-O14 LNP or lung-SORT LNP via four i.v. injections at a total RNA dose of 1 mg kg^{-1}. On day 7, lungs were collected to determine the indels of *TTR* by NGS. **d**, Flow cytometry analysis of ZsGreen1$^+$ cells within defined cell-type populations of the spleen after Cre mRNA delivery ($n = 3$ biologically independent samples). Cre mRNA (5 μg per mouse) was delivered into Ai6 mice by spleen-tropic MC3/12T-O14 LNP or spleen-SORT LNP via i.v. injection. On day 2, mice were euthanized and spleens were collected for analysis. **e**–**g**, SARS-CoV-2 Spike mRNA vaccine delivery (**e**) and antibody responses ($n = 3$ biologically independent samples) (**f**,**g**). C57BL/6 mice were i.v. vaccinated twice with spleen-tropic MC3/12T-O14 LNP or spleen-SORT LNP using a prime–boost strategy with a three-week interval. Anti-Spike IgG titres were determined by ELISA (**f**). NAb titres were determined by a lentivirus-based pseudovirus neutralization assay (**g**). The neutralization titre 50% (NT_{50}) was defined as the greatest serum dilution at which the luminescence was reduced by 50% relative to control cells treated with the pseudovirus in the absence of serum. Data are presented as mean ± s.d. In **a**–**d**, **f** and **g**, one-way ANOVA with Tukey's correction was used. Schematic components in **a**–**e** were created with BioRender.com.

stronger and more precise lung and spleen transfection. Moreover, our spleen-tropic MC3/12T-O14 LNP (10:1) showed higher mRNA EE (92.6% versus 46.0%), comparable spleen transfection (1.5×10^8 p s^{-1} versus 1.7×10^8 p s^{-1}) and less off-target expression compared to the previously reported spleen-tropic 30% 18PA-supplemented C12-200 SORT LNP (termed spleen-SORT LNP; Supplementary Table 3 and Supplementary Fig. 18). Further decrease of the weight ratio to 5:1 for MC3/12T-O14 LNP resulted in a low EE of mRNA (~75%) and a reduced splenic signal below 1×10^7 p s^{-1} (Supplementary Table 3 and Supplementary Fig. 19). This weight ratio was thus not considered for subsequent studies. Altogether, these results suggest that 12T-O14 can serve as a supplementary cationic lipid in liver-tropic LNPs to develop potent lung-tropic or spleen-tropic LNPs via simple alterations of the LNP formulation (Fig. 5e).

AID-lipid enables liver-tropic LNPs to transfect non-liver cells

Inspired by the superior ability of 12T-O14 to selectively redirect liver-tropic LNP to lung or spleen, we next examined the transfection of specific cell types in these organs using an activatable Cre/loxP Ai6 reporter mouse model[39]. Following LNP delivery of Cre recombinase-encoded mRNA (Cre mRNA), the translated Cre protein can cut the STOP cassette, therefore turning on the expression of ZsGreen1 in transfected cells (Fig. 6a). We first confirmed that a strong ZsGreen1 signal was detected in lung sections of lung-tropic MC3/12T-O14 LNP (40:1)-treated mice and in spleen sections of spleen-tropic MC3/12T-O14 LNP (10:1)-treated mice (Supplementary Figs. 20 and 21). We also observed weak ZsGreen1 signal in lung sections of lung-SORT LNP-treated mice and a strong ZsGreen1 signal in spleen sections of spleen-SORT LNP-treated mice. Next, we analysed the transfected cell populations using flow cytometry. Lung-tropic MC3/12T-O14 LNP was able to deliver mRNA to ~6% of total cells and primarily to endothelial cells (ECs, ~60%) in the lung (Fig. 6b and Supplementary Fig. 22), which was more efficient than the lung-SORT LNP. Recently, there has been a growing interest in genome editing through the co-delivery of Cas9 mRNA and sgRNA, as exemplified by Intellia's LNP-mediated liver transthyretin (*TTR*) knockout[40], yet few studies have successfully used this combination to knock out an endogenous gene in the lung[37,41]. We next tested the potential of lung-tropic MC3/12T-O14 LNP to co-deliver Cas9 mRNA and sgRNA for gene editing. *TTR* was selected as a model editing target, and the generation of insertions and deletions (indels) was quantified by next-generation sequencing (NGS). Our lung-tropic MC3/12T-O14 LNP induced ~2.5% *TTR* indels in the lung at a total RNA dose of 1 mg kg^{-1}, which was higher than that induced by lung-SORT LNP (~1.1%; Fig. 6c). Importantly, no pulmonary damage was observed in these edited mice (Supplementary Fig. 23). As expected, liver-tropic MC3 LNP was unable to edit *TTR* in the lung (indels <0.05%), despite it inducing ~6% *TTR* indels in the liver (Supplementary Fig. 24). These results suggest that 12T-O14 expands the potential utility of liver-tropic LNPs for targeted mRNA delivery and gene editing in the lung.

We also analysed the transfected splenocytes after systemic delivery of Cre mRNA using spleen-tropic MC3/12T-O14 LNP. This LNP formulation mainly transfected splenic antigen-presenting cells (APCs), including ~15% of macrophages and ~10% of dendritic cells (DCs; Fig. 6d and Supplementary Fig. 25), which was similar to spleen-SORT LNP. Because there is growing interest in delivering mRNA vaccines to splenic APCs, as exemplified by BioNTech's RNA-LPX system[38,42], we next explored this potential in spleen-tropic MC3/12T-O14 LNP. SARS-CoV-2 Spike mRNA was chosen as a model antigen-encoded mRNA, which enabled us to determine the quality of adaptive immune responses based on the serum anti-Spike IgG titre and SARS-CoV-2 pseudovirus NAb titre. After the prime and boost immunization of spleen-tropic MC3/12T-O14 LNP vaccine (Fig. 6e), the average anti-Spike IgG titre and NAb titre in mice reached 9.9×10^5 and 1.0×10^4, respectively, comparable to those in mice vaccinated with spleen-SORT LNP vaccine (Fig. 6f,g) and higher than those in mice vaccinated with 12T-O14 LNP vaccine or SM-102 LNP vaccine via i.m. injection (Fig. 4b and Supplementary Fig. 16). These results demonstrate the potential of our spleen-tropic MC3/12T-O14 LNP for splenic APC-targeted mRNA vaccine delivery.

Conclusions

In summary, we have developed a T-MCR that could enable fast and facile synthesis of AID-lipids. Such T-MCR methodology broadens the scope of the modular design and synthesis of cationic lipids, which could greatly accelerate the development and study of cationic lipids. We also discovered a distinct head (or tail)–ring-alkyl aniline that can generally produce potent lipids. Mechanistic studies provided insights that the benzene ring facilitates endosomal disruption by aiding the cationic lipid to adopt a more conical shape. The versatile AID-lipid 12T-O14 not only enabled local delivery of mRNA vaccines and systemic delivery of mRNA therapeutics, but also mediated liver-tropic LNPs to selectively deliver gene editors to the lung and mRNA vaccines to the spleen. Therefore, AID-lipids hold potential for aiding the development of mRNA-based vaccines as well as protein replacement and gene-editing therapeutics in target tissues.

Online content

Any methods, additional references, Nature Portfolio reporting summaries, source data, extended data, supplementary information, acknowledgements, peer review information; details of author contributions and competing interests; and statements of data and code availability are available at https://doi.org/10.1038/s41557-024-01557-2.

References

1. Han, X., Mitchell, M. J. & Nie, G. Nanomaterials for therapeutic RNA delivery. *Matter* **3**, 1948–1975 (2020).
2. Chaudhary, N., Weissman, D. & Whitehead, K. A. mRNA vaccines for infectious diseases: principles, delivery and clinical translation. *Nat. Rev. Drug Discov.* **20**, 817–838 (2021).
3. Xiao, Y. et al. Emerging mRNA technologies: delivery strategies and biomedical applications. *Chem. Soc. Rev.* **51**, 3828–3845 (2022).
4. Hou, X., Zaks, T., Langer, R. & Dong, Y. Lipid nanoparticles for mRNA delivery. *Nat. Rev. Mater.* **6**, 1078–1094 (2021).
5. Zhang, H. et al. Rational design of anti-inflammatory lipid nanoparticles for mRNA delivery. *J. Biomed. Mater. Res. A* **110**, 1101–1108 (2022).
6. Han, X. et al. An ionizable lipid toolbox for RNA delivery. *Nat. Commun.* **12**, 7233 (2021).
7. Zhang, Y., Sun, C., Wang, C., Jankovic, K. E. & Dong, Y. Lipids and lipid derivatives for RNA delivery. *Chem. Rev.* **121**, 12181–12277 (2021).
8. Eygeris, Y., Gupta, M., Kim, J. & Sahay, G. Chemistry of lipid nanoparticles for RNA delivery. *Acc. Chem. Res.* **55**, 2–12 (2022).
9. Sabnis, S. et al. A novel amino lipid series for mRNA delivery: improved endosomal escape and sustained pharmacology and safety in non-human primates. *Mol. Ther.* **26**, 1509–1519 (2018).
10. Zhang, X. et al. Functionalized lipid-like nanoparticles for in vivo mRNA delivery and base editing. *Sci. Adv.* **6**, eabc2315 (2020).
11. Maier, M. A. et al. Biodegradable lipids enabling rapidly eliminated lipid nanoparticles for systemic delivery of RNAi therapeutics. *Mol. Ther.* **21**, 1570–1578 (2013).
12. Cornebise, M. et al. Discovery of a novel amino lipid that improves lipid nanoparticle performance through specific interactions with mRNA. *Adv. Funct. Mater.* **32**, 2106727 (2022).
13. Hajj, K. A. et al. Branched-tail lipid nanoparticles potently deliver mRNA in vivo due to enhanced ionization at endosomal pH. *Small* **15**, e1805097 (2019).
14. Akinc, A. et al. A combinatorial library of lipid-like materials for delivery of RNAi therapeutics. *Nat. Biotechnol.* **26**, 561–569 (2008).
15. Semple, S. C. et al. Rational design of cationic lipids for siRNA delivery. *Nat. Biotechnol.* **28**, 172–176 (2010).

16. Jayaraman, M. et al. Maximizing the potency of siRNA lipid nanoparticles for hepatic gene silencing in vivo. *Angew. Chem. Int. Ed.* **51**, 8529–8533 (2012).
17. Whitehead, K. A. et al. Degradable lipid nanoparticles with predictable in vivo siRNA delivery activity. *Nat. Commun.* **5**, 4277 (2014).
18. Love, K. T. et al. Lipid-like materials for low-dose, in vivo gene silencing. *Proc. Natl Acad. Sci. USA* **107**, 1864–1869 (2010).
19. Miao, L. et al. Delivery of mRNA vaccines with heterocyclic lipids increases anti-tumor efficacy by STING-mediated immune cell activation. *Nat. Biotechnol.* **37**, 1174–1185 (2019).
20. Altinoglu, S., Wang, M. & Xu, Q. Combinatorial library strategies for synthesis of cationic lipid-like nanoparticles and their potential medical applications. *Nanomedicine* **10**, 643–657 (2015).
21. Espeel, P., Goethals, F., Driessen, F., Nguyen, L.-T. T. & Du Prez, F. E. One-pot, additive-free preparation of functionalized polyurethanes via amine-thiol-ene conjugation. *Polym. Chem.* **4**, 2449–2456 (2013).
22. Zhou, K. et al. Modular degradable dendrimers enable small RNAs to extend survival in an aggressive liver cancer model. *Proc. Natl Acad. Sci. USA* **113**, 520–525 (2016).
23. Quek, J. Y., Davis, T. P. & Lowe, A. B. Amidine functionality as a stimulus-responsive building block. *Chem. Soc. Rev.* **42**, 7326–7334 (2013).
24. Lv, H., Zhang, S., Wang, B., Cui, S. & Yan, J. Toxicity of cationic lipids and cationic polymers in gene delivery. *J. Control. Release* **114**, 100–109 (2006).
25. Tousignant, J. D. et al. Comprehensive analysis of the acute toxicities induced by systemic administration of cationic lipid:plasmid DNA complexes in mice. *Hum. Gene Ther.* **11**, 2493–2513 (2000).
26. Gilleron, J. et al. Image-based analysis of lipid nanoparticle-mediated siRNA delivery, intracellular trafficking and endosomal escape. *Nat. Biotechnol.* **31**, 638–646 (2013).
27. Patel, S. et al. Naturally-occurring cholesterol analogues in lipid nanoparticles induce polymorphic shape and enhance intracellular delivery of mRNA. *Nat. Commun.* **11**, 983 (2020).
28. Yan, J. et al. Nanomaterials-mediated co-stimulation of toll-like receptors and CD40 for antitumor immunity. *Adv. Mater.* **34**, e2207486 (2022).
29. Tenzer, S. et al. Rapid formation of plasma protein corona critically affects nanoparticle pathophysiology. *Nat. Nanotechnol.* **8**, 772–781 (2013).
30. Pollard, C. et al. Type I IFN counteracts the induction of antigen-specific immune responses by lipid-based delivery of mRNA vaccines. *Mol. Ther.* **21**, 251–259 (2013).
31. Brito, L. A. et al. A cationic nanoemulsion for the delivery of next-generation RNA vaccines. *Mol. Ther.* **22**, 2118–2129 (2014).
32. Prieve, M. G. et al. Targeted mRNA therapy for ornithine transcarbamylase deficiency. *Mol. Ther.* **26**, 801–813 (2018).
33. Baden, L. R. et al. Efficacy and safety of the mRNA-1273 SARS-CoV-2 vaccine. *N. Engl. J. Med.* **384**, 403–416 (2021).
34. Bartesaghi, S. et al. Subcutaneous delivery of FGF21 mRNA therapy reverses obesity, insulin resistance and hepatic steatosis in diet-induced obese mice. *Mol. Ther. Nucleic Acids* **28**, 500–513 (2022).
35. Gimeno, R. E. & Moller, D. E. FGF21-based pharmacotherapy—potential utility for metabolic disorders. *Trends Endocrinol. Metab.* **25**, 303–311 (2014).
36. Loughrey, D. & Dahlman, J. E. Non-liver mRNA delivery. *Acc. Chem. Res.* **55**, 13–23 (2022).
37. Cheng, Q. et al. Selective organ targeting (SORT) nanoparticles for tissue-specific mRNA delivery and CRISPR-Cas gene editing. *Nat. Nanotechnol.* **15**, 313–320 (2020).
38. Kranz, L. M. et al. Systemic RNA delivery to dendritic cells exploits antiviral defence for cancer immunotherapy. *Nature* **534**, 396–401 (2016).
39. Tombacz, I. et al. Highly efficient $CD4^+$ T cell targeting and genetic recombination using engineered $CD4^+$ cell-homing mRNA-LNPs. *Mol. Ther.* **29**, 3293–3304 (2021).
40. Gillmore, J. D. et al. CRISPR-Cas9 in vivo gene editing for transthyretin amyloidosis. *N. Engl. J. Med.* **385**, 493–502 (2021).
41. Liu, S. et al. Membrane-destabilizing ionizable phospholipids for organ-selective mRNA delivery and CRISPR-Cas gene editing. *Nat. Mater.* **20**, 701–710 (2021).
42. Rojas, L. A. et al. Personalized RNA neoantigen vaccines stimulate T cells in pancreatic cancer. *Nature* **618**, 144–150 (2023).

[1]Department of Bioengineering, University of Pennsylvania, Philadelphia, PA, USA. [2]Key Laboratory of RNA Innovation, Science and Engineering, CAS Center for Excellence in Molecular Cell Science, Shanghai Institute of Biochemistry and Cell Biology, Chinese Academy of Sciences, University of Chinese Academy of Sciences, Shanghai, China. [3]Department of Medicine, University of Pennsylvania, Philadelphia, PA, USA. [4]Penn Institute for RNA Innovation, Perelman School of Medicine, University of Pennsylvania, Philadelphia, PA, USA. [5]Department of Bioengineering, George Mason University, Fairfax, VA, USA. [6]Department of Biomedical Sciences, School of Veterinary Medicine, University of Pennsylvania, Philadelphia, PA, USA. [7]Gene Therapy Program, Perelman School of Medicine, University of Pennsylvania, Philadelphia, PA, USA. [8]Department of Chemistry, Case Western Reserve University, Cleveland, OH, USA. [9]Abramson Cancer Center, Perelman School of Medicine, University of Pennsylvania, Philadelphia, PA, USA. [10]Institute for Immunology, Perelman School of Medicine, University of Pennsylvania, Philadelphia, PA, USA. [11]Cardiovascular Institute, Perelman School of Medicine, University of Pennsylvania, Philadelphia, PA, USA. [12]Institute for Regenerative Medicine, Perelman School of Medicine, University of Pennsylvania, Philadelphia, PA, USA. [13]Center for Cellular Immunotherapies, Perelman School of Medicine, University of Pennsylvania, Philadelphia, PA, USA. [14]Center for Precision Engineering for Health, University of Pennsylvania, Philadelphia, PA, USA. [15]These authors contributed equally: Xuexiang Han, Mohamad-Gabriel Alameh, Ningqiang Gong, Lulu Xue. ✉e-mail: dreww@upenn.edu; mjmitch@seas.upenn.edu

Methods

Materials

Amines, oleyl alcohol and linoleyl alcohol were purchased from Sigma Aldrich, Tokyo Chemical Industry (TCI) and Ambeed. The 2-iminothiolane hydrochloride, acrylates, acryloyl chloride and triethylamine (TEA) were obtained from Sigma Aldrich. Mouse IL-6 uncoated ELISA, mouse TNF-α uncoated ELISA, LysoTracker Deep Red and 3,3′-dioctadecyloxacarbocyanine perchlorate (DiO) were bought from Invitrogen. The 1,2-dioleoyl-*sn*-glycero-3-phosphoethanolamine (DOPE), 1,2-distearoyl-*sn*-glycero-3-phosphocholine (DSPC), 1,2-dioleoyl-3-trimethylammonium-propane (chloride salt; DOTAP), 1,2-di-*O*-octadecenyl-3-trimethylammonium propane (chloride salt; DOTMA), 1,2-dimyristoyl-rac-glycero-3-methoxypolyethylene glycol-2000 (DMG-PEG 2000), 1,2-dioleoyl-*sn*-glycero-3-phosphate (sodium salt; 18PA) and cholesterol were obtained from Avanti Polar Lipids. DLin-MC3-DMA, SM-102 and C12-200 were purchased from MedChem Express. Cas9 mRNA (5moU, #L-7206) was purchased from TriLink. Green fluorescent protein siRNA (#P-002048-01-20) was obtained from Horizon Discovery. Highly modified sgRNA targeting mouse *TTR* (guide no. G211) was chemically synthesized by AxoLabs (Supplementary Table 4)[43].

mRNA synthesis

Codon-optimized SARS-CoV-2 di-proline-modified Spike sequence, firefly Luciferase sequence, Cre recombinase sequence or human FGF21 sequence were cloned into an mRNA production plasmid with optimized 3′ and 5′ untranslated regions and a 101 polyA tail, in vitro-transcribed in the presence of 1-methyl-pseudouridine modified nucleoside, co-transcriptionally capped using CleanCap technology (TriLink) and cellulose-purified to remove double-stranded RNAs[44]. Purified mRNA was ethanol-precipitated, washed, re-suspended in nuclease-free water, and subjected to quality control (electrophoresis, dot blot, endotoxin content and transfection into human DCs). All mRNAs were stored at −20 °C until use.

Synthesis of oleyl acrylate (O18a) and linoleyl acrylate (O18b)

Oleyl alcohol or linoleyl alcohol (1 mmol, 1 equiv.) in 10 ml of CH_2Cl_2 was treated with TEA (3 mmol, 3 equiv.) and acryloyl chloride (1.5 mmol, 1.5 equiv.) at 0 °C for 30 min and then at r.t. overnight. The mixture was diluted with CH_2Cl_2 and washed with brine twice. The organic layer was dried over $MgSO_4$, filtered, and concentrated in vacuo. The residue was purified by a CombiFlash NextGen 300+ chromatography system (Teledyne ISCO) with gradient elution from hexane to 80:20 hexane/ethyl acetate, and the desired fractions were collected as colourless oil (yield > 90%). **O18a** was confirmed by MS and NMR. MS-ESI: calculated for $C_{21}H_{38}O_2$: 322.53, found $[M + H]^+$ = 323.51; ^{1}H NMR (400 MHz, CDCl3) δ: 6.40 (dd, J = 17.3, 1.5 Hz, 1H), 6.12 (dd, J = 17.3, 10.4 Hz, 1H), 5.81 (dd, J = 10.4, 1.6 Hz, 1H), 5.41–5.28 (m, 2H), 4.15 (t, J = 6.8 Hz, 2H), 2.01 (q, J = 6.5 Hz, 4H), 1.74–1.61 (m, 2H), 1.43–1.21 (m, 22H), 0.88 (t, J = 6.7 Hz, 3H). **O18b** was confirmed by MS and NMR. MS-ESI: calculated for $C_{21}H_{36}O_2$: 320.52, found $[M + H]^+$ = 321.51; ^{1}H NMR (400 MHz, CDCl3) δ: 6.40 (dd, J = 17.3, 1.5 Hz, 1H), 6.12 (dd, J = 17.3, 10.4 Hz, 1H), 5.81 (dd, J = 10.4, 1.5 Hz, 1H), 5.44–5.27 (m, 4H), 4.15 (t, J = 6.7 Hz, 2H), 2.77 (t, J = 6.4 Hz, 2H), 2.05 (q, J = 6.9 Hz, 4H), 1.74–1.59 (m, 2H), 1.45–1.22 (m, 16H), 0.89 (t, J = 6.7 Hz, 3H).

High-throughput synthesis of AID-lipids

Amine, excessive 2-iminothiolane hydrochloride, excessive acrylate and TEA were dissolved in ethanol in a 1.5-ml Eppendorf tube. All tubes were put on a floating rack and sonicated in an ultrasonic cleaner (Branson M2800) for 1 h at r.t. and at a frequency of 40 kHz. The yield was typically over 80%. Take 12T-O14 as an example: 8 mg of amine 12 (1 equiv.) and 7 mg of 2-iminothiolane hydrochloride (1.5 equiv.) were dissolved in 500 µl ethanol, followed by the addition of 12 mg of acrylate tail **O14** (1.25 equiv.) and 7 mg of TEA (2 equiv.). All crude products were diluted with ethanol to prepare the stock solutions (40 mg ml^{-1}) for LNP preparation.

Purification and characterization of 12T-O14

To purify the top-performing AID-lipid 12T-O14, its crude product was separated using a CombiFlash NextGen 300+ chromatography system with gradient elution from CH_2Cl_2 to 75:22:3 CH_2Cl_2/MeOH/NH_4OH (aq), and the desired fractions were collected as a white solid (yield 84%). 12T-O14 was characterized by MS and NMR. MS-ESI: calculated for $C_{37}H_{66}N_2O_2S$: 603.01, found $[M + H]^+$ = 603.73; ^{1}H NMR (400 MHz, MeOD) δ: 7.43–7.35 (m, 2H), 7.30–7.23 (m, 2H), 4.11 (t, J = 6.6 Hz, 2H), 2.86 (t, J = 7.0 Hz, 2H), 2.82–2.63 (m, 8H), 2.13 (p, J = 7.2 Hz, 2H), 1.66 (dtt, J = 13.0, 6.6, 3.8 Hz, 4H), 1.46–1.22 (m, 36H), 0.92 (t, J = 6.7 Hz, 6H); ^{13}C NMR (100 MHz, MeOD) δ: 173.17, 168.73, 144.88, 132.04, 130.72, 125.61, 65.25, 35.83, 35.04, 32.61, 32.39, 31.87, 31.17, 30.11, 30.08, 30.04, 29.98, 29.92, 29.79, 29.77, 29.67, 29.06, 27.49, 27.09, 26.35, 23.05, 13.75.

LNP formulation and optimization

For high-throughput in vitro and in vivo screening, AID-LNPs were prepared by pipette mixing the ethanolic phase containing AID-lipid, DOPE, cholesterol and DMG-PEG with an aqueous phase (10 mM citrate buffer, pH 3) containing mRNA at a volume ratio of 1:3 and diluted in culture medium or 1× PBS for cell or animal treatment, respectively. The weight ratio of AID-lipid, DOPE, cholesterol, DMG-PEG and mRNA was 16:10:10:3:1.6.

To optimize the LNP formulation, pipette-mixed LNPs with different weight ratios of 12T-O14, cholesterol, DOPE, DMG-PEG and mRNA were tested and screened in vitro and in vivo, and an optimized weight ratio of 16:15:10:3:1.6 was chosen for further studies.

To formulate 12T-O14 LNP and DOTAP LNP by microfluidic mixing, the ethanol phase containing lipids was mixed with the aqueous phase containing mRNA at a flow rate of 1:3 in a microfluidic chip device[45]. LNPs were dialysed against 1× PBS in a 20-kDa molecular-weight-cutoff cassette for 2 h, filtered through a 0.22-µm filter and stored at 4 °C. DiO-labelled LNPs were obtained by mixing DiO (1 mol% of total lipids) with LNPs before dialysis.

SM-102 (or MC3) LNP was formulated by SM-102, DSPC, cholesterol and DMG-PEG at a molar ratio of 50:10:38.5:1.5 using microfluidic mixing. MC3/12T-O14 LNP was formulated with MC3, DSPC, cholesterol, DMG-PEG and 12T-O14 at a molar ratio of 25:5:19.25:0.75:50 at a total lipids:mRNA weight ratio of 40, 20, 10 or 5. Specifically, lung-targeted MC3/12T-O14 LNP and MC3/DOTAP SORT LNP (lung-SORT LNP)[37] with a total lipids:mRNA weight ratio of 40 was formulated by pipette mixing. After dialysis, these LNPs were directly used without filtration. 30% 18PA C12-200 SORT LNP (spleen-SORT LNP) was formulated using microfluidic mixing as previously reported[37].

Characterization

^{1}H NMR and ^{13}C NMR spectra were recorded using a Bruker 400-MHz NMR spectrometer. LC-MS was performed on a Waters Acquity LC-MS system equipped with UV–vis and MS detectors. The hydrodynamic size, PDI and zeta potential of the LNPs were measured using a Zetasizer Nano ZS90 set-up (Malvern Instruments). The morphology of the LNPs was characterized by a cryo-electron microscope (Titan Krios, Thermo Fisher). The mRNA encapsulation efficiency and the pK_a of LNPs were determined using a modified Quant-iT RiboGreen RNA assay (Invitrogen) and a 6-(*p*-toluidinyl)naphthalene-2-sulfonic acid (TNS) assay, respectively[46,47].

Cell-culture and animal studies

HepG2 cells were obtained from American Type Culture Collection (ATCC #HB-8065) and maintained in Dulbecco's modified Eagle medium (DMEM) supplemented with 10% fetal bovine serum (FBS), 100 U ml^{-1} penicillin and 100 µg ml^{-1} streptomycin. ACE-II-expressing human embryonic kidney 293 (HEK-293/ACE-II) cells were purchased

from Takara (#631289) and maintained in RPMI-1640 medium. Cells were cultured at 37 °C in a humidified incubator of 5% CO_2, and routinely tested for mycoplasma contamination.

All animal protocols were approved by the Institutional Animal Care and Use Committee (IACUC) of University of Pennsylvania (#806540), and animal procedures were performed in accordance with the Guidelines for Care and Use of Laboratory Animals at the University of Pennsylvania. C57BL/6 female mice (6–8 weeks, 18–20 g) were purchased from Jackson Laboratory. Ai6 (RCL-ZsGreen) mice on a C57BL/6J background were purchased from Jackson Laboratory (#007906) and bred homozygous in-house. C57BL/6 and Ai6 mice were housed in a specific-pathogen-free animal facility at ambient temperature (22 ± 2 °C), air humidity of 40–70% and a 12-h dark/12-h light cycle.

High-throughput in vitro screening of AID-LNPs

HepG2 cells were seeded into 96-well plates at a density of 5,000 per well overnight, and mLuc-loaded AID-LNPs (15 ng per well) were used to treat the cells for 24 h. Luciferase expression was evaluated by a Luciferase Reporter 1000 Assay System (Promega, #E4550), and cell viability was measured using a CellTiter-Glo Luminescent Cell Viability Assay (Promega, #G7572) according to the manufacturer's protocols.

In vivo screening of AID-LNPs

Mice were anaesthetized with 2.5% isoflurane, and mLuc-loaded AID-LNPs (2 μg of mRNA in 40 μl of PBS) were injected into the left or right gastrocnemius muscle using a 29-G needle. After 4 h, mice were intraperitoneally injected with D-luciferin potassium salt (150 mg kg^{-1}), and bioluminescence imaging was performed on an IVIS imaging system (PerkinElmer).

Molecular dynamics simulations

Lipid dynamics simulations of 12T-O14, 4T-O14 and DOTAP were optimized with the CHARMm force field[48]. The lipid simulations were run with up to 4,000 steps to achieve the energy-minimized structures. All bonds containing intermolecular interactions were constrained using the Smart Minimizer algorithm (that is, 1,000 steps of steepest descent with a root-mean-squared (r.m.s.) gradient of 3 and conjugate gradient minimization). The overall r.m.s. gradient tolerance was set to 0.01. The Momany–Rone method was assigned for partial charge estimation using Discovery Studio 2018 (Accelrys)[48]. The dimensionless packing parameter p of a lipid molecule was calculated as $p = V/(AL)$ based on its van der Waals molecule volume (V), the cross-sectional area of the polar head (A) and average tail length (L)[28]. V, A and L were derived from the optimized conformation of the lipid as well as the estimated atomic van der Waals radius[49].

Cellular uptake

HepG2 cells were seeded into 35-mm glass-bottom dishes for 24 h and treated with DiO-labelled LNPs (300 ng mRNA ml^{-1}) for 2 h. Afterwards, cells were stained with LysoTracker Deep Red (100 nM) for 45 min and Hoechst 33342 (10 μg ml^{-1}) for 5 min. Images were taken immediately using a confocal laser scanning microscope (LSM 710, Zeiss).

Haemolysis assay

Mouse red blood cells (RBCs) were isolated and washed twice with 1× PBS by centrifugation at 700g for 5 min. The RBCs were then diluted in PBS (pH 7.4 or 6.0) to a 4% vol/vol RBC solution and incubated with LNPs at a concentration of 3 μg mRNA ml^{-1} at 37 °C for 1 h. The RBC solution was centrifuged at 700g for 5 min, and 100 μl of the supernatant was transferred into a 96-well plate. The absorption at 540 nm was determined with a plate reader. Positive and negative controls were carried out with 0.1% Triton-X and 1× PBS, respectively.

Local mRNA delivery

Mice were i.m. injected with SARS-CoV-2 Spike mRNA-loaded LNPs (2 μg mRNA in 40 μl of PBS) twice using a prime–boost strategy with a three-week interval. Blood was collected into serum separator tubes (BD, #365967) via the retro-orbital route. Serum was acquired after centrifugation at 10,000g for 5 min and stored at −20 °C until use.

Systemic mRNA delivery

Mice were i.v. injected with 100 μl of mLuc-loaded LNPs (2 μg mRNA per mouse). In vivo bioluminescence imaging was performed at 4 h post-injection as described above. The mice were euthanized, and major organs (heart, liver, spleen, lung and kidney) were acquired for ex vivo bioluminescence imaging immediately.

For systemic FGF21 mRNA delivery, mice were i.v. injected with 100 μl of FGF21 mRNA-loaded LNPs (5 μg mRNA/mouse). Serum was collected at 0, 6 and 24 h post-injection and stored at −20 °C until analysis of FGF21 by ELISA (R&D, #DF2100). Liver function was examined by measuring the activities of serum aspartate aminotransferase (Cayman, #701640) and serum alanine aminotransferase (Cayman, #700260). Thirteen mouse cytokines were examined using a LEGENDplex multi-analyte flow assay kit (BioLegend, #740621) according to the manufacturer's instructions. Major organs were collected at 24 h post-injection and processed for histological examination after stained with haematoxylin and eosin (H&E).

Lung-targeted and spleen-targeted mRNA delivery

mLuc delivery. To use 12T-O14 as a fifth component to navigate liver-tropic LNP to transfect the lung, MC3/12T-O14 LNP with a total lipid:mRNA weight ratio of 40 was i.v. injected at a dose of 2 μg mLuc per mouse. Lung-targeted MC3/DOTAP LNP was used as a control. To optimize MC3/12T-O14 LNP formulation for spleen targeting, MC3/12T-O14 LNPs with different total lipids:mRNA weight ratios (40, 20, 10 or 5) were i.v. injected at a dose of 2 μg mLuc per mouse. In vivo and ex vivo bioluminescence imaging were performed at 4 h post-injection.

Cre mRNA delivery and flow cytometry. Lung-tropic MC3/12T-O14 LNP with a total lipids:mRNA weight ratio of 40 was i.v. injected into Ai6 mice at a dose of 5 μg Cre mRNA per mouse. Lung-SORT LNP was used as a control. Mice were euthanized on day 2, and lungs were collected. The lungs were digested with 1.5 mg ml^{-1} collagenase A (Sigma, #COLLA-RO) and 0.1 mg ml^{-1} DNase I (Sigma, #10104159001) for 1 h, filtered through 70-μm cell strainers in complete DMEM, centrifuged, and the RBCs were lysed in ACK lysis buffer to obtain a clear single-cell suspension. The samples were stained with live/dead aqua for 5 min, blocked using anti-mouse CD16/32 antibody for 20 min, and strained extracellularly for 30 min using antibodies. The cells were washed in FACs buffer and fixed with 300 μl (1%) paraformaldehyde. The samples were analysed on a BD LSR II system equipped with four laser lines and 18 photomultiplier tubes. The gating strategy for endothelial cells ($PECAM^+$), macrophages ($CD11b^+$), monocytes ($CD64^+$), neutrophils ($Ly6G^+$) and DCs ($CD11c^+$), as well as the antibody list and catalogue numbers, are provided in Supplementary Fig. 22.

Spleen-tropic MC3/12T-O14 LNP with a total lipids:mRNA weight ratio of 10 was i.v. injected into Ai6 mice at a dose of 5 μg Cre mRNA per mouse. Spleen-SORT LNP was used as a control. Mice were euthanized at 2 d post-injection, and spleens were collected. The spleens were processed, filtered through 70-μm cell strainers in complete DMEM, centrifuged, and RBCs were lysed in ACK lysis buffer to obtain a clear single-cell suspension. The samples were stained and analysed as described above. The gating strategy for leukocytes ($CD45^+$), macrophages ($CD11b^+$), monocytes ($CD64^+$), neutrophils ($Ly6G^+$) and DCs ($CD11c^+$), as well as the antibody list and catalogue numbers, are provided in Supplementary Fig. 25.

Lung-targeted Cas9 mRNA/sgTTR co-delivery. Cas9 mRNA and sgTTR (4:1, wt:wt) were encapsulated into MC3/12T-O14 LNP at a total lipids:RNA weight ratio of 40. C57BL/6 mice were i.v. administrated with this lung-tropic MC3/12T-O14 LNP on days 0, 1, 3 and 4 (four injections; in total,

1 mg kg^{-1}). On day 7, lungs were collected to determine the indels of *TTR* by NGS or processed for histological examination after staining with H&E. Lung-SORT LNP was used as a positive control for lung gene editing. MC3 LNP was used as a positive control for liver gene editing and as a negative control for lung gene editing. For *TTR* on-target DNA sequencing, DNA was extracted using the Qiagen Puregene Tissue Kit (#158063) and quantified using a NanoDrop 2000 system. Polymerase chain reaction (PCR) amplification of the *TTR* target site was carried out using Q5 High-Fidelity DNA Polymerase (New England Biolabs, #M0491) and the following primer sequences: mTTR-exon2-F, 5′-CGGTTTACTCTGACCCATTTC-3′ and mTTR-exon2-R, 5′-GGGCTTTCTACAAGCTTACC-3′. Deep sequencing of the *TTR* amplicons and determination of the on-target indel frequency were performed essentially as described, except that 150-bp pair-end reads were produced[50].

Spleen-targeted mRNA vaccine delivery. SARS-CoV-2 Spike mRNA was encapsulated into MC3/12T-O14 LNP at a total lipids:mRNA weight ratio of 10. C57BL/6 mice were i.v. administrated with this spleen-tropic MC3/12T-O14 LNP twice (2 μg of mRNA each) using a prime–boost strategy with a three-week interval. Spleen-SORT LNP was used as a control. Serum was collected for analysis.

Determination of anti-Spike IgG titres using ELISA

First, 96-well clear polystyrene high bind Stripwell microplates (Corning) were coated overnight with 1 μg ml^{-1} purified SARS-CoV-2 His tagged Spike protein (Sino Biological, #40589-V08H8). The plates were washed once with wash buffer (0.05% Tween-20 in PBS), then blocked for 2 h at r.t. using a solution of heat-inactivated, IgG-depleted, protease-free bovine serum albumin (BSA, 2% wt/vol, in PBS). After blocking, the plates were washed three times, and mouse sera were serially diluted in the blocking solution and incubated for 2 h at r.t. The plates were washed three times before the addition of horseradish peroxidase-conjugated anti-mouse secondary antibody specific to IgG (1:10,000, Abcam, #ab97040) in blocking buffer. The plates were incubated for 1.5 h, then washed three times before the addition of 100 μl per well of 3,3′,5,5′-tetramethylbenzidine substrate for 8 min. The reaction was stopped by adding 50 μl of 2 N sulfuric acid, and the absorbance was measured at 450 nm using a SpectraMax 190 microplate reader. The Spike-specific IgG end-point dilution titre was defined as the highest dilution of serum to give an optical density (OD) greater than the cutoff OD value determined using the Frey method[51].

SARS-CoV-2 pseudovirus neutralization assay

A pseudovirus neutralization assay was performed using a lentivirus-based system expressing the D614G Spike protein (Integral Molecular, #RVP-702L). HEK-293/ACE-II cells were seeded at a density of 20,000 cells per well in 96-well plates overnight. Serum samples were serially diluted in RPMI-1640 medium and incubated with an equivalent volume (1:1, vol/vol) of lentivirus-based pseudovirus expressing Renilla Luciferase (50 foci forming units). The lentivirus-serum mixture was incubated at 37 °C for 1 h to allow interaction between neutralizing antibodies and pseudovirus particles. The mixture (100 μl) was then added to the HEK-293/ACE-II cells and incubated for 48 h. Luciferase expression was evaluated by the Renilla-Glo Luciferase Assay System (Promega, #E2710) according to the manufacturer's protocols. The neutralization titre 50% (NT_{50}) was determined as the greatest serum dilution at which the luminescence was reduced by 50% relative to control cells treated with the pseudovirus in the absence of serum. NT_{50} titres for each sample were measured in two technical replicates performed on separate days.

Statistical analysis

Data are presented as mean ± s.d. Student's *t*-test or one-way analysis of variance (ANOVA) followed by Tukey's test were used for comparison between two groups or among multiple groups, respectively. Probability $P < 0.05$ was considered to be statistically significant.

Reporting summary

Further information on research design is available in the Nature Portfolio Reporting Summary linked to this article.

Data availability

All relevant data supporting the findings of this study are available within the paper and the Supplementary Information. Source data are provided with this paper.

References

43. Finn, J. D. et al. A single administration of CRISPR/Cas9 lipid nanoparticles achieves robust and persistent in vivo genome editing. *Cell Rep.* **22**, 2227–2235 (2018).
44. Baiersdorfer, M. et al. A facile method for the removal of dsRNA contaminant from in vitro-transcribed mRNA. *Mol. Ther. Nucleic Acids* **15**, 26–35 (2019).
45. Han, X. et al. Ligand-tethered lipid nanoparticles for targeted RNA delivery to treat liver fibrosis. *Nat. Commun.* **14**, 75 (2023).
46. Riley, R. S. et al. Ionizable lipid nanoparticles for in utero mRNA delivery. *Sci. Adv.* **7**, eaba1028 (2021).
47. Billingsley, M. M. et al. Ionizable lipid nanoparticle-mediated mRNA delivery for human CAR T cell engineering. *Nano Lett.* **20**, 1578–1589 (2020).
48. Momany, F. A. & Rone, R. Validation of the general purpose QUANTA® 3.2/CHARMm® force field. *J. Comput. Chem.* **13**, 888–900 (1992).
49. Mantina, M., Chamberlin, A. C., Valero, R., Cramer, C. J. & Truhlar, D. G. Consistent van der Waals radii for the whole main group. *J. Phys. Chem. A* **113**, 5806–5812 (2009).
50. Wang, L. et al. Meganuclease targeting of PCSK9 in macaque liver leads to stable reduction in serum cholesterol. *Nat. Biotechnol.* **36**, 717–725 (2018).
51. Frey, A., Di Canzio, J. & Zurakowski, D. A statistically defined endpoint titer determination method for immunoassays. *J. Immunol. Methods* **221**, 35–41 (1998).

Acknowledgements

M.J.M. acknowledges support from a US National Institutes of Health (NIH) Director's New Innovator Award (DP2 TR002776), a Burroughs Wellcome Fund Career Award at the Scientific Interface (CASI), a US National Science Foundation CAREER Award (CBET-2145491) and an American Cancer Society Research Scholar Grant (RSG-22-122-01-ET). M.J.M. and J.M.W. acknowledge support from a sponsored research agreement with iECURE. We acknowledge S. Steimle from Beckman Center for Cryo Electron Microscopy at the University of Pennsylvania for help with characterizing the morphology of LNPs. We acknowledge UPenn Gene Therapy Program NAT Core for sequencing service and thank K. Martins from UPenn GTP for processing the NGS data. We thank Y. Zhong from State Key Laboratory of Natural and Biomimetic Drugs, Peking University for providing access to computing resources in molecular dynamic simulation studies. The funders had no role in study design, data collection and analysis, decision to publish or preparation of the manuscript.

Author contributions

X.H., M.-G.A., N.G., L.X. and M.J.M. designed experiments. X.H., M.-G.A., N.G., L.X., G.Z., C.C.W., G.B., R.E.-M. and G.D. performed experiments. X.H., M.-G.A., N.G. and L.X. analysed data. X.H., M.-G.A. and M.J.M. wrote the paper. All authors discussed and edited the paper content.

Competing interests

X.H. and M.J.M. are inventors on a patent filed by the Trustees of the University of Pennsylvania (US provisional patent application no. 63/589,051, filed 10 October 2023) describing the

amidine-incorporated degradable lipid nanoparticle technology in this paper. In accordance with the University of Pennsylvania policies and procedures and our ethical obligations as researchers, we report that D.W. is named on patents that describe the use of nucleoside-modified mRNA as a platform to deliver therapeutic proteins and vaccines. M.J.M., X.H., D.W. and M.-G.A. are also named on patents describing the use of lipid nanoparticles, and lipid compositions for nucleic acid delivery and vaccination. We have disclosed those interests fully to the University of Pennsylvania, and we have in place an approved plan for managing any potential conflicts arising from licensing of our patents. J.M.W. is a paid advisor to and holds equity in iECURE, Passage Bio and the Center for Breakthrough Medicines (CBM). He also holds equity in the former G2 Bio asset companies. He has sponsored research agreements with Amicus Therapeutics, CBM, Ceva Santé Animale, Elaaj Bio, FA212, Foundation for Angelman Syndrome Therapeutics, former G2 Bio asset companies, iECURE and Passage Bio, which are licensees of Penn technology. J.M.W. and C.C.W. are inventors on patents that have been licensed to various biopharmaceutical companies and for which they may receive payments. The other authors declare no competing interests.

Additional information

Supplementary information The online version contains supplementary material available at https://doi.org/10.1038/s41557-024-01557-2.

Correspondence and requests for materials should be addressed to Drew Weissman or Michael J. Mitchell.

Peer review information *Nature Chemistry* thanks Anna Blakney and the other, anonymous, reviewer(s) for their contribution to the peer review of this work.

nature portfolio

Corresponding author(s): Michael Mitchell

Last updated by author(s): Mar 31, 2024

Reporting Summary

Nature Portfolio wishes to improve the reproducibility of the work that we publish. This form provides structure for consistency and transparency in reporting. For further information on Nature Portfolio policies, see our Editorial Policies and the Editorial Policy Checklist.

Statistics

For all statistical analyses, confirm that the following items are present in the figure legend, table legend, main text, or Methods section.

n/a	Confirmed	
☐	☒	The exact sample size (*n*) for each experimental group/condition, given as a discrete number and unit of measurement
☐	☒	A statement on whether measurements were taken from distinct samples or whether the same sample was measured repeatedly
☐	☒	The statistical test(s) used AND whether they are one- or two-sided *Only common tests should be described solely by name; describe more complex techniques in the Methods section.*
☒	☐	A description of all covariates tested
☐	☒	A description of any assumptions or corrections, such as tests of normality and adjustment for multiple comparisons
☐	☒	A full description of the statistical parameters including central tendency (e.g. means) or other basic estimates (e.g. regression coefficient) AND variation (e.g. standard deviation) or associated estimates of uncertainty (e.g. confidence intervals)
☐	☒	For null hypothesis testing, the test statistic (e.g. *F*, *t*, *r*) with confidence intervals, effect sizes, degrees of freedom and *P* value noted *Give P values as exact values whenever suitable.*
☒	☐	For Bayesian analysis, information on the choice of priors and Markov chain Monte Carlo settings
☒	☐	For hierarchical and complex designs, identification of the appropriate level for tests and full reporting of outcomes
☒	☐	Estimates of effect sizes (e.g. Cohen's *d*, Pearson's *r*), indicating how they were calculated

Our web collection on statistics for biologists contains articles on many of the points above.

Software and code

Policy information about availability of computer code

Data collection	ZEN2010, Bruker 400 MHz NMR spectrometer, Zetasizer Nano ZS90, IVIS specturm
Data analysis	Statistical analysis was performed on Graphpad Prism 7.0, flow cytometry data were analyzed on FlowJo software package (Flowjo V10), 1H NMR spectrum was analyzed by MestReNova x64, confocal images were analyzed by Zen 2011 software and molecular simulation was performed on BIOVIA Discovery Studio 2018.

For manuscripts utilizing custom algorithms or software that are central to the research but not yet described in published literature, software must be made available to editors and reviewers. We strongly encourage code deposition in a community repository (e.g. GitHub). See the Nature Portfolio guidelines for submitting code & software for further information.

Data

Policy information about availability of data

All manuscripts must include a data availability statement. This statement should provide the following information, where applicable:

- Accession codes, unique identifiers, or web links for publicly available datasets
- A description of any restrictions on data availability
- For clinical datasets or third party data, please ensure that the statement adheres to our policy

All relevant data supporting the findings of this study are available within the paper and the Supplementary Information. Source data are provided with this paper.

Human research participants

Policy information about studies involving human research participants and Sex and Gender in Research.

Reporting on sex and gender	No human participants were involved in this study.
Population characteristics	No human participants were involved in this study.
Recruitment	No human participants were involved in this study.
Ethics oversight	No human participants were involved in this study.

Note that full information on the approval of the study protocol must also be provided in the manuscript.

Field-specific reporting

Please select the one below that is the best fit for your research. If you are not sure, read the appropriate sections before making your selection.

☒ Life sciences ☐ Behavioural & social sciences ☐ Ecological, evolutionary & environmental sciences

For a reference copy of the document with all sections, see nature.com/documents/nr-reporting-summary-flat.pdf

Life sciences study design

All studies must disclose on these points even when the disclosure is negative.

Sample size	No statistical methods were used to determine the sample size in the study. The sample sizes are clearly described in each figure legend. The sample size were determined by allowable error size, accuracy, resources, and need for statistical analysis (generally n>=3 throughout all the studies). For initial screening, n=2 was used for rapid and cost-efficient screening of lipid candidates.
Data exclusions	No animals and/or data were excluded.
Replication	All experiments were repeated for at least three times and experimental findings were reproducible.
Randomization	For in vivo study, animal groups were randomized by body weight. For other experiments, all samples were randomly allocated into experimental groups, as there was no covariate in the study design.
Blinding	All the investigators were blinded to group allocation during data collection and analysis.

Reporting for specific materials, systems and methods

We require information from authors about some types of materials, experimental systems and methods used in many studies. Here, indicate whether each material, system or method listed is relevant to your study. If you are not sure if a list item applies to your research, read the appropriate section before selecting a response.

Materials & experimental systems

n/a	Involved in the study
☐	☒ Antibodies
☐	☒ Eukaryotic cell lines
☒	☐ Palaeontology and archaeology
☐	☒ Animals and other organisms
☒	☐ Clinical data
☒	☐ Dual use research of concern

Methods

n/a	Involved in the study
☒	☐ ChIP-seq
☐	☒ Flow cytometry
☒	☐ MRI-based neuroimaging

Antibodies

Antibodies used	Anti-mouse CD16/32 antibody (1:100, #101319, BioLegend), Pacific Blue anti-mouse CD11c antibody (1:100, #117321, BioLegend), APC anti-mouse PECAM-1 antibody (1:100, #17-0311-82, Thermofisher), APC anti-mouse CD45 antibody (1:100, #MCD4505, BioLegend), PE/Cy7 anti-mouse Ly6G antibody (1:100, #127617, BioLegend), PE/CF594 anti-mouse CD64 antibody (1:100, #139319, BioLegend), PerCP/Cy5.5 anti-mouse CD11b antibody (1:100, #101227, BioLegend), HRP-conjugated anti-mouse secondary antibody (1:10,000, #ab97040, Abcam)

Validation	All antibodies were verified by the supplier and each lot has been quality tested. All the antibodies used are from commercial sources and have been validated by the vendors. Validation data are available on the manufacturer's website.

Eukaryotic cell lines

Policy information about cell lines and Sex and Gender in Research

Cell line source(s)	HepG2 cells were obtained from American Type Culture Collection (ATCC), and ACE-II expressing human embryonic kidney 293 (HEK-293/ACE-II) cells were purchased from Takara. These cell lines were tested negative for mycoplasma in University of Pennsylvania cell center.
Authentication	A short tandem repeat DNA profiling method was used to authenticate the cell lines and the results were compared with reference database. Moreover, no mycoplasma contamination was detected in the above cell lines.
Mycoplasma contamination	These cells were tested for mycoplasma contamination. No mycoplasma contamination was found.
Commonly misidentified lines (See ICLAC register)	HepG2 cell line and HEK-293/ACE-II are not listed in the database.

Animals and other research organisms

Policy information about studies involving animals; ARRIVE guidelines recommended for reporting animal research, and Sex and Gender in Research

Laboratory animals	All animal protocols were approved by the Institutional Animal Care and Use Committee (IACUC) of University of Pennsylvania (#806540), and animal procedures were performed in accordance with the Guidelines for Care and Use of Laboratory Animals at the University of Pennsylvania. C57BL/6 female mice (6-8 weeks, 18-20 g) were purchased from Jackson Laboratory. Ai6 (RCL-ZsGreen) mice on C57BL/6J background were purchased from Jackson Laboratory (#007906) and bred homozygous in-house. C57BL/6 and Ai6 mice were housed in a specific-pathogen-free animal facility at ambient temperature (22 ± 2 °C), air humidity 40%–70% and 12-h dark/12-h light cycle.
Wild animals	No wild animal was used in this study.
Reporting on sex	Female mice were used for this study. Sex should not affect the results.
Field-collected samples	The study did not involve samples collected from field.
Ethics oversight	All animal experiment protocols were reviewed and approved by the institutional animal care and use committee of the University of Pennsylvania.

Note that full information on the approval of the study protocol must also be provided in the manuscript.

Flow Cytometry

Plots

Confirm that:

☒ The axis labels state the marker and fluorochrome used (e.g. CD4-FITC).

☒ The axis scales are clearly visible. Include numbers along axes only for bottom left plot of group (a 'group' is an analysis of identical markers).

☒ All plots are contour plots with outliers or pseudocolor plots.

☒ A numerical value for number of cells or percentage (with statistics) is provided.

Methodology

Sample preparation	Spleens were collected, processed, filtered using a 70 µm cell strainers in complete RPMI-1640, centrifuged, and red blood cells lysed in ACK lysis buffer. Single-cell suspensions were obtained and stained with antibodies according to the manufacturer's protocols, and then analyzed by flow cytometry. Lungs were digested with 1.5 mg/mL Collagenase A (Sigma, #COLLA-RO) and 0.1 mg/mL DNase I (Sigma, #10104159001) for 1 h, filtered through a 70 µm cell strainers in complete DMEM, centrifuged, and red blood cells lysed in ACK lysis buffer to obtain a clear single cell suspension. Cells were stained with antibodies according to the manufacturer's protocols, and then analyzed by flow cytometry.
Instrument	BD LSR II
Software	FlowJo software package (Flowjo V10)
Cell population abundance	The absolute cells >= 10000 were analyzed for fluorescent intensity in the defined gate.
Gating strategy	In general, cells were first gated on FSC/SSC. Singlet cells were gated using FSC-H and FSC-A. Dead cells were then excluded

Gating strategy	and further surface and intracellular antigen gating was performed on the live cell population (See supplementary infomation).

☒ Tick this box to confirm that a figure exemplifying the gating strategy is provided in the Supplementary Information.